

INTERNAL FRICTION IN ZIRCONIUM  
AND ZIRCONIUM ALLOYS

INTERNAL FRICTION IN THE REGION OF THE  
GRAIN BOUNDARY PEAKS IN PURE ZIRCONIUM  
AND DILUTE ZIRCONIUM ALLOYS

By

R.C. Robinson

A Thesis

Submitted to the School of Graduate Studies  
in Partial Fulfillment of the Requirements

for the Degree

Master of Engineering

McMaster University

December, 1976

MASTER OF ENGINEERING (1977)  
(Engineering Physics)

McMASTER UNIVERSITY  
Hamilton, Ontario

TITLE: Internal Friction in The Region of The Grain Boundary  
Peaks in Pure Zirconium and Dilute Zirconium Alloys

AUTHOR: R.C. Robinson, B. Eng. (McMaster University)

SUPERVISOR: Dr. I.G. Ritchie

NUMBER OF PAGES: v, 66

## ABSTRACT

Internal friction, in the region of the grain boundary peaks, has been examined in nominally pure zirconium and dilute zirconium alloys. Experimental observations were made using both torsion and reed internal friction pendulums. The effect of various heat treatments on the peaks were investigated. Strain amplitude dependent damping in the region of the Low Temperature Peak was observed. A qualitative model is presented to explain the experimental observations.

## ACKNOWLEDGEMENTS

I sincerely thank Dr. I.G. Ritchie for his invaluable help and assistance throughout all phases of this work. I would also like to thank Dr. R. Dutton and Dr. J. Robinson for their helpful comments on the revision of my manuscript. Also, I would like to acknowledge the excellent technical assistance of K.W. Sprungmann and H. Schmidt. I would also like to express my gratitude to Atomic Energy of Canada Limited for allowing me to work at Whiteshell Nuclear Research Establishment.

## TABLE OF CONTENTS

	Page
1. INTRODUCTION	1
2. REVIEW OF THEORY	
2.1 The Grain Boundary Peaks .....	3
2.2 Background Internal Friction .....	14
3. RESULTS OF EXPERIMENTS USING THE TORSION PENDULUM	
3.1 The Apparatus .....	16
3.2 The Experiments .....	18
3.3 Discussion of Torsion Results .....	22
Grain Boundary Peaks	
3.4 Background .....	25
4. REED PENDULUM EXPERIMENTS	
4.1 The Apparatus .....	27
4.2 Experiments .....	27
4.3 Discussion of Reed Pendulum Experiments .....	29
5. CONCLUSIONS AND SUGGESTIONS FOR FURTHER WORK	36
References .....	38
Figure Captions .....	40
Tables 1 and 2 .....	42
Figures .....	43-66

## INTRODUCTION

Since the first identification by Ke<sup>1</sup> of maxima in high temperature internal friction experiments, due to the presence of grain boundaries, a large number of similar observations have been reported. However, a detailed explanation of the basic mechanism has not yet been developed. In this report, we further investigate the occurrence of high temperature damping maxima.

It should be noted that as many as three distinct peaks in the internal friction spectrum have been attributed to grain boundaries. They are usually referred to as a L.T.P. (low temperature peak) between  $0.3$  and  $0.4T_m$  (where  $T_m$  is the melting temperature) an I.T.P. (intermediate temperature peak) at  $0.5T_m$  and, in some cases, a H.T.P. (high temperature peak) around  $0.8T_m$ . In conjunction with the peaks, a monotonically increasing background has also been observed. The size and position of these peaks have been found to be sensitive to the grain size, the purity of the metal, and the prior heat and mechanical treatments of the specimens used in the tests.

Subsequent to these observations, a number of models have been postulated. A grain boundary sliding model was first presented by Zener<sup>2</sup> and Ke<sup>3,4</sup> to account for these phenomena. This model was later modified by Raj and Ashby<sup>5</sup>,

and by Mosher and Raj<sup>6</sup> to explain the effect of impurities on the peaks. Several qualitative models have also been suggested which include the following various effects: the migration of grain boundary protrusions<sup>7</sup>, damping by dislocations at grain boundaries<sup>8</sup>, and grain boundary migration<sup>9</sup>. A quantitative model involving the reversible climb and glide of dislocations in the grain boundaries and lattice has also been postulated.<sup>10</sup>

In this report, internal friction in the region of the grain boundary peaks in nominally pure zirconium and dilute zirconium alloys is examined. The experimental observations present in this report have been made using both torsion and reed internal friction pendulums similar to those described in references 13 and 14. The effects of various heat treatments on the peaks have been investigated. In particular, strain amplitude dependent damping in the region of the peaks was observed. It should be noted that strain amplitude dependent damping peaks were observed throughout the entire temperature range investigated. These peaks are interpreted in terms of a dislocation unpinning model.



## 2. REVIEW OF THEORY

### 2.1 The Grain Boundary Peaks

Experimental evidence of an internal friction (I.F.) peak peculiar to polycrystalline materials was first obtained by Ke (1947a)<sup>1</sup> in his work on single crystal and polycrystalline aluminum. A maximum in the I.F. was observed by Ke in the vicinity of 300°C during a testing of polycrystalline aluminum in torsional vibrations at 0.8Hz. This peak was not present in "Single Crystal" aluminum. Ke attributed this peak to the relaxation of shear stress across a viscous grain boundary.

The model used by Ke assumes a flat boundary of thickness  $b$  and area of order  $d^2$  where  $d$  is the grain diameter with a characteristic viscosity  $\eta$ . Such a boundary is shown schematically in fig. 2.1. With the onset of a stress across the boundary, the crystal lattice initially deforms elastically. However, since the grain boundary material is assumed to be viscous, grain 1 starts to slide over grain 2 under the influence of the applied shear stress to build up opposing stresses at the ends of the boundaries and into grains 3 and 4. This relaxation process comes to a halt when the shear stress has dropped to zero across most of the length of the boundary. This process produces the offset  $\Delta X$  between grain 1 and grain 2. At low stress levels, the distortion at the edges is assumed

to be purely elastic. This distortion at the edges provides the necessary elastic-restoring force to reduce  $\Delta X$  to zero upon removal of the applied stress. This process is anelastic since it is recoverable upon the removal of the applied stress and since the additional strain from sliding is accumulated and discharged with a characteristic relaxation time. This sliding process then produces an elastic after-effect and indicates that an idealized sample containing a collection of identical boundaries would correspond to the standard anelastic solid. Thus, this process should exhibit a relaxation peak in the damping spectrum with a characteristic relaxation time  $\tau$ .

The relaxation time  $\tau$  can be determined by considering the kinetics of the relaxation process to be dependent on an effective viscosity co-efficient  $\eta$  at the grain boundary. By analogy with the standard anelastic solid, the rate of change of the slip distance  $\Delta X$ , with time, will be proportional to its deviation from its final equilibrium slip distance  $\overline{\Delta X}$  so,

$$\frac{d(\Delta X)}{dt} = (\overline{\Delta X} - \Delta X) / \tau \quad 2.1$$

where  $\tau$  is the characteristic relaxation time, the initial slip velocity for  $\Delta X = 0$  is then:

$$v(0) = \overline{\Delta X} / \tau \quad 2.2$$

For a boundary of width  $b$  under an initially uniform shear stress  $\sigma$ ,  $v(0)$  may also be written as:

$$v(0) = \sigma b / \eta \quad 2.3$$

To reduce the shear stresses at the boundary to zero, the local anelastic strain at the boundary  $\Delta X/d$  must relieve the elastic strains; therefore, we have;

$$\frac{\Delta X}{d} = \sigma / G \quad 2.4$$

Where  $G$  is the elastic modulus. From equations 2.2, 2.3, and 2.4, we obtain;

$$\tau = \frac{d \cdot \eta}{bG} \quad 2.5$$

If one then assumes a simple Arrhenius type relationship<sup>9</sup> for the dependence of the viscosity with temperature i.e.

$$\eta = \eta_0 \exp(Q/kT) \quad 2.6$$

then the temperature dependence of  $\tau$  is;

$$\tau = \frac{\eta_0}{dG} \exp(Q/RT) \quad 2.7$$

Where  $Q$  is the activation energy of the process and  $\eta_0$  is the viscosity at absolute zero temperature.

Determination of the activation energy for equation 2.7 depends on the atomistic processes involved in sliding at the grain boundary. Ke considered the boundary to consist of islands of atoms of good fit and islands of disordered atoms. Thus, the sliding process would be that of forcing disordered atoms past the islands of good fit. The activation energy of this simplified process is then that of self-diffusion since Ke does not differentiate between the type and concentration of imperfections in the boundary and in the grain. Mott (1948)<sup>15</sup> also considered the boundary to be a transition region consisting of islands of good lattice fit between the adjacent grains separated by regions of bad lattice fit between the adjacent grains. However, slip, according to Mott, would involve the disordering of atoms around each of the islands. If  $n$  atoms are disordered around each island, Mott showed that the activation energy of the process would be;

$$Q = nL \quad 2.8$$

where  $L$  is the latent heat of fusion per atom. Ke found some agreement between the activation energy of self-diffusion and the activation energy measured from the shift of the peak with frequency. If Ke's results are interpreted using 2.8 an  $n$  of approximately 14 is obtained.

It is not clear how the simple model used by

Ke would explain the effect of impurities on the so-called grain boundary peaks. The addition of both substitutional and interstitial impurities have caused marked changes in the so-called pure peak (L.T.P.) and evolution of a second and sometimes third impure peak (I.T.P. and H.T.P.)<sup>16, 17</sup>. The height and position of all these peaks have been shown to be very sensitive to impurity concentration<sup>16, 17</sup>.

An attempt at including the effect of impurities on the grain boundary peaks using a modified sliding model has been made by Mosher and Raj<sup>6</sup>. They incorporated some of the theoretical results obtained from the paper of Raj and Ashby<sup>5</sup> into their own sliding model for grain boundary I.F. They considered a polycrystal containing inclusions in the grain boundaries as shown in fig. 2.2. The inclusions were assumed to be particles of precipitated impurities at the boundaries. As in Ke's model upon onset of the stress, the grains elastically deform and start to slide. However, due to the presence of impurity precipitate particles, the resistance to sliding is greater than in the pure metal case since the boundary has to elastically deform to accommodate sliding across the particles. Mosher and Raj postulate that this elastic deformation is accomplished by the diffusive flux of pure lattice atoms around the particles either by a route through the lattice or along the grain boundary as shown in fig. 2.2. A spring-dashpot model in fig. 2.3 describes the

various parameters which are relevant to the Mosher and Raj model. The spring stiffness describes the total sliding strain available for a given applied stress. The three dashpots describe the viscosities which control the rate at which the sliding can accumulate.  $\eta_B$  is the intrinsic viscosity of a particle-free planar boundary and corresponds to the pure metal grain boundary viscosity measured by Ke in his experiments.  $\eta_{BDIFF}$  and  $\eta_{VDIFF}$  are the additional resistance to sliding introduced by accommodating sliding across the particles by diffusion of atoms.  $\eta_{BDIFF}$  and  $\eta_{VDIFF}$  were calculated by Raj and Ashby<sup>5</sup> and shown to be valid for sliding of bi-crystals<sup>18</sup>. For particles impermeable to diffusion of diameter  $p$  and with interparticle spacing  $\lambda$ , the sliding viscosities are given by:

$$\eta_{BDIFF} = \frac{bKTp^4}{8\Omega\lambda^2} \cdot \frac{1}{bD_b} \quad 2.9$$

$$\eta_{VDIFF} = \frac{b \cdot KT}{1.6 \cdot \Omega} \cdot \frac{p^3}{\lambda^2} \cdot \frac{1}{D_v} \quad 2.10$$

where  $b$  is the grain boundary thickness,  $\Omega$  is the atomic volume; and  $D_B$  and  $D_V$  are the self-diffusion coefficients for grain boundary and volume diffusion. Mosher and Raj have shown that the relaxation time  $\tau$  is given by:

$$\tau = \eta/bB \quad 2.11$$

for a boundary of a general sliding viscosity  $\eta$  where B for an equiaxed grain structure is given by:

$$B = \frac{1}{1.14} \cdot \frac{E}{(1-\nu^2)} \cdot \frac{1}{\bar{d}} \quad 2.12$$

where E and  $\nu$  are Young's Modulus and Poisson's Ratio, respectively and  $\bar{d}$  is the grain size of the polycrystal. For the model shown in fig. 2.3, the dashpot with the highest viscosity will be the rate-controlling step for the relaxation process.

Mosher and Raj showed, by using appropriate numbers for  $D_B$ ,  $D_V$ , and  $\Omega$ , that the viscosity  $\eta_{BDIFF}$  and  $\eta_{VDIFF}$  per boundary thickness (b) is much greater than the pure viscosity  $\eta_B$  for copper. The particle size p and spacing  $\lambda$  was determined metallographically from oxidated Ca-Ge and Cu-S alloys used as specimens in their internal friction experiments. They also showed that in copper  $\eta_{BDIFF}$  is much greater than  $\eta_{VDIFF}$ . They, therefore, used  $\eta_{VDIFF}$  in 2.11 with equation 2.12 and obtained the following:

$$\tau = 0.14 \cdot \frac{KT(1-\nu^2)}{E\Omega} \cdot \frac{p^4 d}{\lambda^2 \delta D_B} \quad 2.13$$

In summary, the model of Mosher and Raj predicts that a grain boundary peak will occur at a higher temperature in an impure metal rather than at the pure metal peak, and this peak will shift in position with particle size, particle spacing, and grain size in accordance with equation 2.13 since  $\tau$  determines the position of this anelastic peak. If

grain boundary diffusion is the rate controlling step, the activation energy for the peak will be that of grain boundary diffusion; and consequently, the activation energy for the peak will be that of self-diffusion if volume diffusion is dominant. Mosher and Raj found agreement between their model and their experimental data.

Leak<sup>9</sup> (1961) found a correlation between the activation energy of the grain boundary peak in pure iron and that of grain boundary self-diffusion. From this observation, he postulated that the grain boundary damping could be associated with grain boundary migration in the form of sub-microscopic grain growth. Qualitatively, this process could lead to anelastic phenomena; however, the necessary elastic-restoring force was not made clear by Leak.

At an elevated temperature, it appears that dislocations travel along grain boundaries (Weirtman 1955<sup>19</sup>, Ishida and McLean 1967<sup>20</sup>, Ashby 1969<sup>21</sup>, Ishida and Liu 1970<sup>22</sup>). As such movement is usually a mixture of glide and climb, sliding of one grain with respect to the other and emission or absorption of vacancies is the result. Roberts and Barrand<sup>8</sup> introduced a dislocation model to explain the L.T.P. in F.C.C. metals and their observed relationship between peak relaxation strength  $\Delta_a$  peak activation energy  $Q_p$ , and  $d_0$  the width of the dissociated dislocation. They postulated that the relaxation peak was due to the reversible motion of dislocations in grain



boundaries. Roberts and Barrand<sup>8</sup> also attempted to explain the influence of grain size and impurities on the L.T.P. in terms of their model. However, the actual elastic-restoring force to create the reversible motion is not clear, and their model is only qualitative.

Recently, a quantitative model for grain boundary peaks, involving glide and climb of dislocations, has been developed by J. Worrigard<sup>10</sup>. The elastic-restoring force is the line tension of a dislocation bowed out between pinning points as shown schematically in fig. 2.4. The anelastic strain is created by the dislocation undergoing climb under the influence of the applied stress. The rate of climb of the dislocation is controlled by the diffusion of vacancies. Thus, the relaxation time would be different if diffusion occurs in the grain boundary compared with diffusion in the lattice.

Worrigard writes the strain rate produced by climb and glide of dislocations as follows:

$$\dot{\epsilon} = \frac{3\beta G\Omega^2}{KTA^2} A \left( \epsilon - \frac{\rho\Lambda^2\sigma}{3\beta G} \right) \quad 2.14$$

Where:  $\rho$  = dislocation density

$\Lambda$  = half mean spacing between pinning points

$J$  = shear modulus

$b$  = Burgers Vector

$K$  = Boltzmann constant

$T$  = absolute temperature

$\Omega$  = vacancy volume

$A$  = factor related to the exact diffusion path and contains the diffusion parameter

$\beta$  = geometric constant such that  $T_e = \beta G b^2$   
( $T_e$  being the line tension).

If we now compare equation 2.13 with the equation of strain rate for a standard anelastic solid which is:

$$\dot{\epsilon} = \frac{1}{\tau} (\epsilon - \sigma \delta G) \quad 2.15$$

we see that the relaxation strength  $\frac{\delta G}{G}$  is given by:

$$\frac{\delta G}{G} = \Delta J = \frac{\rho \Lambda^2}{3\beta}$$

and the relaxation time by:

2.16

$$\tau = \frac{K T \Lambda^3}{3 \beta G \Omega^2 A}$$

for Worrigard,s model. Thus, a relaxation peak with the relaxation strength and relaxation time given by 2.16 should occur in the I.F. Spectrum.

One important aspect of this model is that no assumption is made concerning the nature or position of the dislocations. The only assumption is that dislocations of opposite signs exchange vacancies and are pinned either by point defects or

by other dislocations. The dislocation structure responsible for the relaxation peak may not necessarily be in the grain boundaries but may be in the lattice structure of the grains. This then implies that I.F. peaks, due to dislocation relaxation, may occur in single crystal if an appropriate dislocation structure exists in the crystal.

The activation energy of the dislocation relaxation peaks, however, will change depending on where the diffusion of vacancies takes place. For movement of grain boundaries dislocations, diffusion of vacancies could take place in the boundary. Worrigard has calculated for this case that  $\tau$  is given by:

$$\tau = \frac{KT}{3\beta G\Omega} \cdot \frac{\Lambda^2 \ell}{D_b b} \cdot \sin^2 \phi \cos^2 \phi \quad 2.17$$

and the relaxation magnitude is:

$$\Delta J = \frac{\rho \Lambda^2}{3\beta} \sin^2 \phi \cos \phi \quad 2.18$$

where  $b$  is the boundary width and  $\ell$  being the mean spacing between grain boundary dislocations.  $\phi$  is the angle that the Burgers Vectors of the dislocation makes with the boundary. In this case, the activation energy would be that of grain boundary diffusion since  $D_b$ , the grain boundary diffusion coefficient appears in the expression for  $\tau$ (2.17).

If, however, dislocations in the grain are responsible

for a relaxation process, the vacancies would travel through the crystal lattice from a dislocation acting as a source to one acting as a sink. This mechanism would have a relaxation time given by:

$$\tau = \frac{KT}{6\pi\beta G\Omega} \cdot \Lambda^2 \text{Log} \frac{R}{\ell b} \quad 2.19$$

where:  $R$  is the cut-off parameter and  $\ell$  is the mean spacing between dislocations and  $D_v$  is the co-efficient for diffusion of vacancies in the crystal lattice (self-diffusion). The activation energy in this case is that for self-diffusion.

All the preceding models developed for grain boundary internal friction consider the process to be wholly anelastic in origin. Thus, the internal friction observed is expected to be amplitude independent. Recently, however, amplitude dependent effects have been reported in the vicinity of the grain boundary peak in polycrystalline magnesium.<sup>23</sup> Thus, if the amplitude dependent damping in the region of the grain boundary peak is a general effect, re-examination of all previous reported data would be necessary. Furthermore, any model developed for grain boundary peaks would have to include the possibility of amplitude dependence when extended to higher strain amplitudes.

## 2.2 Background Internal Friction

The rise in background of internal friction in the high temperature region has usually been thought to arise from the thermal activation of dislocations.<sup>24</sup> This background has been shown to vary exponentially with temperature according to an

Arrheneous relationship of the form:

$$\Delta = A \exp(-H/RT) \quad 2.20$$

where: H is the activation energy, R the gas constant, T the absolute temperature, and A a structure sensitive term. Furthermore, the frequency dependence of the high temperature background damping is thought to be given by:

$$\Delta = \frac{A}{f^n} \exp(-H/RT) \quad 2.21$$

where F is the frequency and n is usually in the range of 1 to 2.

## RESULTS OF EXPERIMENTS USING THE TORSION PENDULUM

### 3.1 The Apparatus

An inverted torsion pendulum operating in a frequency range around 1Hz was used. The apparatus is the same as that described by Putman, Ritchie and Sprungman<sup>14</sup>. In fig. 3.1 is shown a schematic diagram of the instrumentation used in the torsion system. The torsion pendulum and the vacuum chamber is shown in fig. 3.2. Vacuum was maintained at less than  $10^{-3}$  torr throughout all experiments.

Damping was measured using two techniques. The electrical energy required to maintain the oscillations of the pendulum at a constant amplitude was used as one measure of damping. Free decay of the oscillations was also used, where the damping can be determined from the Log Dec given by:

$$\text{Log Dec} = \Delta = \text{Log} \left( \frac{A_0}{A_1} \right) = \frac{1}{N} \text{Log} \left( \frac{A_0}{A_n} \right) \quad 3.1$$

where  $A_0$ ,  $A_1$ , and  $A_n$  are the first, second, and  $n^{\text{th}}$  amplitude of the free decay and  $N$  is the number of oscillations in between.

In the torsion tests, the latter method was used chiefly to calibrate the drive method. Driving at constant strain amplitude is accomplished through use of a pendulum control circuit. It is shown in reference 14 that the current supplied to the drive coil  $I_0$  is related to  $\Delta$  the Log Dec by:

$$\Delta = \frac{I_0}{K_2 \epsilon G} \quad 3.2$$

where  $K_2$  is a constant,  $\epsilon$  is the surface shear strain amplitude, and  $G$  is the shear modulus. This equation shows that if the pendulum is driven at a constant strain amplitude, the drive current is directly proportional to  $\Delta$  through the constant  $K_2 \epsilon G$ . This constant can then be determined through calibration of drive results against free-decay results. The strain amplitude in the drive mode is controlled by a reference voltage level ( $V_0$ ) with nominal values from 0 to 10V. Each level corresponds to approximately 0.001 of an inch displacement of the inertia arm at the transducer. The strain amplitude of the specimen is then given by<sup>14</sup>:

$$\epsilon = \frac{rX_0}{\ell R} \quad 3.3$$

$$\text{where: } X_0 = cV_0 \quad 3.4$$

and where  $r$  is the radius of the specimen,  $\ell$  is its length, and  $R$  is the radial displacement of the transducer from the axis of the pendulum.  $X_0$  is the displacement of the inertia arm at the transducer and  $c$  is the conversion constant between the reference voltage level  $V_0$  and  $X_0$ . Thus,  $\epsilon$  can then be given by:

$$\epsilon = K_3 V_0 \quad 3.5$$

where: for a given test  $K_3$  is a constant.

### 3.2 The Experiments

The samples tested are listed in table 1 along with their composition and grain size. Micrographs are shown of specimen 1 before and after testing in fig. 3.3. A typical chemical analysis of the marz grade Zr supplied by the manufacturer is shown in table 2. The alloys are prepared from marz grade Zr alloyed with pure elements. These specimens were oxidized to 1% by weight and annealed at 1050°C for 5.2 days. This was thought sufficient for complete homogenization.

The marz grade Zr specimen, 6.03 inches in length with an average diameter of .0343 inches, was mounted and annealed in situ at 750°C for 2 hours to reduce handling strains. Temperature of the specimen was changed and controlled by the apparatus outlined in reference 14. Less than 1°C fluctuations along the length were detected below 600°C. Above 600°C, the temperature differential was slightly larger. The pendulum was driven at a  $V_0$  equal to 4V. This amounts to a constant strain amplitude of  $5.0 \times 10^{-6}$ . The drive current and temperature was monitored on an X-Y recorder yielding a continuous reading for the damping as a function of temperature.

In fig. 3.4, the resulting damping spectrum is shown in a typical warm-up to 750°C. The Log Dec was obtained from the drive current through equations 3.2. The experimental



curve obtained is curve A of fig. 3.4. To estimate a background of the form given by equation 2.20, a plot of  $\ln(\Delta T)$  vs.  $1/T$  was done for curve A of fig. 3.4. This plot is shown in fig. 3.5. A straight line was drawn tangent to several points at low temperatures outside the peak regions. The slope of this line is then the activation energy in equation 2.20 and is equal to 18. kcal./mole in this case. This is then the extrapolated background used in fig. 3.4 to resolve the peaks. This is the procedure used in estimating backgrounds in all experimental curves.

In the experiments of Gacoungnole<sup>12</sup> with Zr, there was evidence of two peaks appearing in the temperature range from 400°C to 800°C, a L.T.P. and an I.T.P. Thus, the experimental curve obtained in these studies was analyzed accordingly. In fig. 3.4, the maximum of the L.T.P. was taken as the maximum of the spectrum after background subtraction. The low temperature side of this maximum was symmetrically reflected to the higher temperature side. Thus, peak C of fig. 3.4 was first obtained, then both peak C and the background were subtracted from curve A. This produced a peak D at 680°C. This procedure is justified since the contribution of the I.T.P. is minimal at the L.T.P. maximum as is the case with fig. 3.4.

The shape of curve A, in fig. 3.4 was that which was generally observed in several warm-ups to 740°C. However, the height of peak C appeared to slightly diminish with each succeeding

run. Also, after an in situ anneal at  $780^{\circ}\text{C}$  for 2 hours and cooling to room temperature, the subsequent warm-up revealed a damping spectrum as shown in curve A of fig. 3.6. Subtraction of a much lower background but with same activation energy and the use of the same resolution technique as before revealed an L.T.P. greatly diminished in height. The peak at higher temperature remained at approximately the same height but was shifted in temperature.

A test of the Zr-Mo-0 alloy sample revealed the damping spectrum shown as curve A of fig. 3.7. After subtraction of the background curve B, a peak at  $482^{\circ}\text{C}$  was resolved, shown by curve C of fig. 3.7, there was no evidence of a I.T.P. The value of the damping at the peak is .0217 in terms of Log Dec which is much smaller than the peak in the marz grade specimen at a similar temperature. The sample was not subjected to an in situ anneal before the recording of curve A. However, after an anneal for 2 hours of  $750^{\circ}\text{C}$ , the peak at  $482^{\circ}\text{C}$  has all but disappeared as shown by curves D and F in fig. 3.7. There appeared to be the emergence of a second peak at higher temperatures ( $800^{\circ}\text{C}$ ) i.e. above the limit of the experimental apparatus.

The testing of the Zr-Y-0 specimen resulted in experimental curve A in fig. 2.8. A peak was observed at  $580^{\circ}\text{C}$  at a frequency of 1.68Hz. No prior in situ anneal was done; and after recording of curve A, the sample was rapidly cooled to

room temperature. Weights were installed on the inertia arm of the pendulum to reduce the frequency of oscillations to 0.46Hz at room temperature. In the subsequent warm-up, the damping spectrum recorded is shown in fig. 3.9. Two major differences were noted in this warm-up in comparison to the previous one at higher frequency. The background subtracted was higher by a factor of approximately 3.3 and the peak, although approximately the same height, was shifted. From a shift with frequency, the relaxation time ( $\tau$ ) for a relaxation peak can be determined by the following method:  $\tau$  the relaxation time is given by:

$$\tau = \frac{1}{\omega} = \tau_0 \exp(Q/RT_p) \quad 3.6$$

where  $Q$  is the activation energy,  $R$  is the gas constant, and  $T_p$  the absolute temperature at the peak position. Then, for  $\omega_1$  at  $T_{p1}$  and  $\omega_2$  at  $T_{p2}$  we have from 3.6:

$$\frac{\frac{1}{\omega_1}}{\frac{1}{\omega_2}} = \frac{\tau_0 \exp(Q/RT_{p1})}{\tau_0 \exp(Q/RT_{p2})} \quad 3.8$$

or

$$Q = R \ln \frac{\omega_2}{\omega_1} \left\{ \frac{1}{T_{p1}} - \frac{1}{T_{p2}} \right\}^{-1} \quad 3.9$$

where  $\tau_0$  is assumed independent of  $\omega$ . For the shift in temperature of the L.T.P. for 1.68Hz and 0.461Hz an activation energy of 63 kcal./mole was found. If the peak is a true Debye peak (i.e. the standard anelastic solid model holds),

the peak will have a single relaxation time  $\tau$ . For such a peak, the activation energy can be calculated from the peak half width by:

$$Q_{HW} = \frac{2.635 R}{\Delta(T^{-1})} \quad 3.10$$

where  $\Delta(T^{-1})$  is the peak half width in the inverse absolute temperature spectrum. Using 3.10 a  $Q_{HW}$  of 25 kcal./mole was obtained from the peak in 2.8 and  $Q_{HW}$  of 32. kcal./mole for the peak in fig. 2.9. The difference between the two activation energies is within experimental error. However, both activation energies are significantly lower than 63 kcal./mole obtain from the peak shift. This difference between  $Q_{HW}$  and  $Q$  peak shift indicates that this process does not have a single relaxation time, but a distribution of relaxation times. This point is discussed further in the next section. The activation energy of the background in both cases was approximately 22 kcal./mole. In addition, there was evidence of a peak around 400°C which is thought to be the oxygen s - i peak as predicted by Ritchie et.al.<sup>25</sup>

### 3.3 Discussion of Torsion Results Grain Boundary Peaks.

As can be seen in figs. 3.1, 3.2, 3.4, after subtraction of a suitable background, a peak in the 500 to 600° region was found in all specimens tested. This peak was present regardless of the purity of the material. However, the peak height is

diminished in alloy specimens. In specimens 1 and 3, as a result of a high temperature anneal, the peak is greatly reduced.

No detectable change in the grain size before and after testing was found in the alloys. However, slight grain growth did occur in the Marz Grade sample. Specimen 2 was not subjected to a high temperature anneal to ensure that the minimum change took place in the peak in order to determine the activation energy with minimum error.

$K_e^1$  showed that the height of the peak predicted by the sliding model, is independent of grain size as long as the grain size was less than the specimen's dimensions. Since only minimal grain growth occurred in the pure specimen, and since the grain size was much less than the specimen's dimension, the peak heights should have been of constant height. Thus, the drastic reduction in the L.T.P. of pure Zr after a high temperature anneal is difficult to explain in terms of the sliding model. Furthermore, appearance of a peak in a similar temperature region in the alloy samples behaving in a similar manner as in the pure Zr sample suggests that the alloy peaks are of the same origin as the so-called pure peak. This also contradicts the extended sliding model of Mosher and Raj<sup>6</sup> since the G.B. peaks predicted for impure samples with precipitate particles at the boundary should occur at a much higher temperature than the pure peaks. It appears then that neither the

original sliding model nor the extended sliding model can be used as an explanation for the L.T.P. observed in this study.

In his thesis, Gacougnolle<sup>10</sup> found a similar peak at 530°C in commercial zirconium as was found in specimen 1. The activation energy of that peak was given by him to be 60 ±10 kcal./mole which agrees well with the activation energy of the peak in specimen 2 in this temperature region. He also found the peak diminishes after annealing in the beta phase. He postulated that the peak was due to a dislocation relaxation similar to that predicted by the Worrigard model. However, because the activation energy was that close to volume self-diffusion<sup>10</sup> for pure Zr, he concluded that the dislocation structure responsible occurred in the lattice. Thus, the heat treatment changed the peak characteristics since it changed the dislocation structure responsible for the peak.

A similar explanation seems acceptable for the L.T.P. observed in this study on Zr and Zr alloys. The L.T.P. then is not necessarily present due to grain boundaries although the presence of grain boundaries may effect the density and characteristic of the dislocation structure in the grains. The dislocation structure responsible seems to be stable below 750°C but prolonged annealing at a higher temperature drastically changes the structure; thus, changing the nature of the peaks. Mechanically induced strains on the solid would also tend to change the dislocation structure. This is probably why even

after an anneal at 1050°C for 5.2 days the alloys showed an I.T.P. since handling strains were introduced upon mounting of the specimen and no in situ anneal was done prior to initial testing. The distribution in  $\tau$ , found earlier, is probably due to the distribution of dislocation lengths in the dislocation structure since the relaxation time for a dislocation relaxation is governed by equation 2.16 which contains a  $\Lambda^3$  term.

The I.T.P. in marz grade zirconium, however, does not seem sensitive to heat treatment. This peak was not present in the alloys. The emergence of a high temperature peak 780°C was present in the spectrum of specimen 3. These peaks could be the grain boundary precipitate peaks predicted by the Mosher and Raj's<sup>6</sup> sliding model. Some shift was found in the I.T.P. (700°C) in specimen 1, which could possibly be due to the slight grain growth that occurred; this is predicted by the sliding model. However, not enough experimental evidence is present to specify the nature of these higher temperature peaks.

### 3.4 Background

A plot of  $\ln(\Delta T)$  vs.  $1/T$  yields a straight line which is tangent to the experimental curves at a low temperature outside the peak area. The activation energies from the slope of the line ranged from 18 kcal./mole to 22 kcal./mole. This is similar to the activation energy obtained by Gacougnolle<sup>10</sup> in his thesis from use of equation 2.20. The  $1/f^n$  dependence

predicted by equation 2.21 also seems to hold since the background change is a factor of 3.3 which is approximately the same ratio of the two frequencies 3.03. Thus,  $n$  would be approximately 1 which is similar to what has been observed elsewhere.<sup>24</sup>



## 4. REED PENDULUM EXPERIMENTS

### 4.1 The Apparatus

The reed pendulum apparatus used is described in detail by Ritchie et. al.<sup>13</sup> A schematic diagram of the system is shown in fig. 4.1 and 4.2. Damping can be measured at a constant strain amplitude through monitoring the drive current needed to sustain constant amplitude. Damping can also be measured from the Log Dec given in equation 3.1 from free decay. Data logging in free decay is facilitated through the use of a small computer with amplitude and period monitoring capabilities. The amplitude and period of each cycle of a free decay can be measured accurately. Thus, the damping and modulus defect can be obtained as a function of nominal strain amplitude of free decay ( $V_0$ ). The nominal strain amplitude can be converted to real strain amplitude through equation 3.5 re-written here for convenience as:  $\epsilon = V_0 K_3$ .

where  $K_3$  is  $1.361 \times 10^{-6}$  for specimen 4 and  $1.255 \times 10^{-6}$  for specimen 5. The above is the method employed in experiments throughout this report where damping is measured as a function of strain amplitude.

### 4.2 Experiment

Marz grade zirconium specimens, in the form of rectangular reeds of approximately 3 cm. in length, were tested using the reed pendulum. The frequency of operation was in the region of 4Hz.

The specimens are listed in table 1 as specimens 4 and 5.

Specimen 5 contained a fairly uniform grain structure. However, there existed a large distribution of grain sizes in specimen 4 containing some fairly large grains. Thus, the grain size in table 1 for specimen 4 is only an approximate average.

The specimens were heated at a rate of  $2^{\circ}\text{C}$  per minute, and free-decay measurements were taken every 10 minutes after the specimen temperature was allowed to stabilize at each temperature for 15 minutes. Less than  $1^{\circ}$  temperature difference throughout the length of the specimens was maintained. Vibration of the specimens was maintained at a constant nominal strain amplitude of  $V_0 = 4$  throughout the warm-up and the stabilisation period. However, for free-decay measurements, the amplitude was increased to  $V_0 = 9$  using the drive system. The amplitude was allowed to stabilise at  $V_0 = 9$  before the drive was switched off, and the ensuing decay monitored as described above.

The result of one such warm-up of specimen 5 is shown in figs. 4.3 through 4.7. A plot of damping vs. strain amplitude in the temperature range of  $413^{\circ}\text{C}$  to  $644^{\circ}\text{C}$  is shown in figs. 4.3, 4.4, 4.5, and 4.6. Amplitude dependence of the damping is apparent throughout this temperature range.

Amplitude dependent damping was also encountered in the testing of specimen 4. Damping vs. strain amplitude curves for specimen 4 are shown in fig. 4.8.

In both specimens, the damping vs. strain amplitude curves changes with temperature, and at some temperatures a

peak is clearly evident in these plots. For specimen 5, an amplitude independent region seems to exist at lower strain amplitude. A plot of the damping for nominal strain amplitude of 1 vs. temperature is shown in fig. 4.7. A curve similar to that obtained in the torsion test for marz grade zirconium is obtained. A similar plot for specimen 4 is shown in fig. 4.9 although an amplitude independent region is not clearly established.

#### 4.3 Discussion of Reed Pendulum Experiments

From figs. 4.3, 4.4, and 4.5, it is seen that the Log Dec was highly amplitude dependent in the strain range investigated. Specifically in the temperature range of the L.T.P. in zirconium (500°C - 650°C), strong amplitude dependence is encountered. There appears, however, to be an amplitude independent region at low strain amplitude ( $<1.4 \times 10^{-6}$ ). The damping in this region is plotted as a function of temperature as curve A in fig. 4.7. This plot yields a damping curve similar to that seen in the torsion experiments. A similar plot for specimen 5 is shown in figs. 4.8 and 4.9.

At higher strain amplitudes ( $>2 \times 10^{-6}$ ), the damping tends to rise steeply at first but then peaks, and in some cases, starts to fall again. A plot of one such peak at 550°C is shown in fig. 4.6. The modulus defect  $\Delta M$  is also shown as the dotted curve of fig. 4.6.  $\Delta M$  is calculated from:

$$M = 1 - \left( \frac{f}{f_0} \right)^2 \quad 4.1$$

where:  $f_0$  is the average frequency at low strain amplitude in the amplitude independent region, and  $f_1$  is the oscillation frequency at the given strain amplitude in the amplitude dependent region. Peaks in damping, as a function of strain amplitude, have been predicted by the Granato-Lucke<sup>26</sup> model for unpinning of dislocations. This model, however, is for unpinning at zero absolute temperature.

It was shown by Lucke and Schlipf<sup>27</sup>, however, that at elevated temperature, the zero temperature model could be used if one replaces the critical mechanical stress for dislocation unpinning by the thermal breakaway stress. In fig. 4.6, the modulus defect  $\Delta M$ , as a function of strain amplitude, rises through the peak to approximately 1/2 the Log Dec at the peak, and then tends to flatten out. This is in agreement with theories of temperature assisted unpinning and not in agreement with zero absolute temperature models. The strain amplitude where these peaks occur is indicative of the critical stress needed for breakaway.

The Granato-Lucke theory yields the following expression:

$$\Delta_{BA} = \frac{T\Delta_0 \Omega L n^3}{\pi L_C} \cdot \frac{3! \Gamma \exp-\Gamma}{RM \epsilon_0 RM \epsilon_0} \quad 4.2$$

for low strain amplitudes. An extension of the Granato-Lucke theory to the high strain side of the unpinning peak has been made by Rogers<sup>29</sup> and recently modified by Ritchie<sup>30</sup> et. al.

to give the following expression:

$$\Delta_{BA} = \frac{T\Delta_0\Lambda L n^2 \cdot 3! \Gamma^2 g(n)}{\pi (RE) \epsilon_0^2} \quad 4.3$$

for high strain amplitude. In these equations, T and R are orientation factors, M is the appropriate elastic modulus for the test (M is Young's modulus in this case), Ln is the dislocation density,  $\epsilon_0$  the characteristic stress for unpinning, and  $\Delta_0 = 8Mb^2 / 3T$  where b is the Burgers vector of the dislocations and T the line tension given by  $T = 1/2Gb^2$ .  $\Delta_{BA}$  and  $\epsilon_0$  are the corresponding values of the logarithmic decrement and the strain amplitude respectively on the breakaway or unpinning peak. n is the average number of pins and g(n) is a function which has been determined numerically by Ritchie et al.<sup>30</sup>

Equation 4.2 shows that plots of  $\ln \Delta_{BA} \epsilon_0$  vs.  $1/\epsilon_0$  for low  $\epsilon_0$  values should give a straight line of slope  $m_1 = -\Gamma/RE$  and intercept  $\ln A_1 = \ln (T\Delta_0 \Lambda L n^3 3! \Gamma) / (\pi L C RE)$ . Similarly equation 4.3 shows that a plot of  $\Delta_{BA}$  vs.  $1/\epsilon_0^2$  at high values of  $\epsilon_0$  should give a straight line of slope  $m_2 = (T\Delta_0 \Lambda L n^2 3! \Gamma^2 g(n)) / (\pi RE^2)$  and intercept  $A_2 = 0$ . Such plots have been done for the peak in fig. 4.6 and is shown in figs. 4.10 and 4.11. From these plots, we obtained  $A_1 = 3.37 \times 10^{-6}$ ,  $m_1 = 11.33 \times 10^{-6}$  and  $m_2 = 3.205 \times 10^{-13}$ . It is also shown in reference (30) that the following relationship holds:

$$\frac{n+1}{g(n)} = \frac{A_1 |m_1|}{m_2} \quad 4.4$$

Where:  $n+1/g(n)$  was determined numerically in ref. (30) as a function of  $n$ , the number of pinning points. Using our parameters  $n+1/g(n)$  was calculated to be 119 from the plot in ref. (30) an  $n$  of approximately 8 was obtained.

Although 8 pinning points per dislocation is reasonable, it is slightly low and is close to the region where the numerical approximation in ref. (30) cease to be good approximations. One reason for obtaining a rather low number of pinning points from the method outlined above could be that the slope  $m_2$ , from the plot of  $\Delta_{BA}$  vs.  $1/\epsilon_0$ , may not be completely due to unpinning even if the plot appears linear. One possible source of error is that the high strain side of the peak may be superimposed on an increasing background due to microplastic generation of dislocations at high strain amplitude. Thus,  $n = 8$  can be treated as a lower limit to the number of breakable pins per dislocation. This calculation, however, supports the validity of the procedure outlined in ref.(30)

The peaks in damping vs. strain amplitude can then be interpreted using the Granato-Lucke model. The peak positions, however, are not constant and tend to shift with temperature. When a plot of the strain amplitude where the peak occurs (which is indicative of the critical breakaway stress) against temperature is superimposed on the low strain damping curve, as done in fig. 4.7, several interesting features become apparent. Three consecutive peaks evolve and sweep through the strain

range moving to lower strain amplitudes at increasing temperature. At low strain amplitude, the first two peaks seem to disappear while the next evolves. This process is seen most clearly in the curve for free decay at  $444^{\circ}\text{C}$  and  $493^{\circ}\text{C}$  of fig. 4.3. However, the last peak does not disappear but starts to move back to higher strain amplitudes after reaching a minimum. From examination of fig. 4.7, this effect apparently co-incides with the peak in damping at low strain amplitude. This effect then appears to possess some intrinsic relationship with the LT.P.

The movement of breakaway peaks to lower strain amplitude can be explained by the sophisticated model of Blair, Hutchison, and Rogers<sup>28</sup>. It can also be explained if one simply assumes that the thermal breakaway stress decreases with increasing temperature, which seems intuitively obvious. However, the return to higher strain amplitudes cannot be accounted for by either model. Thus, curve B and C of fig. 3.7 can be explained by a thermally assisted unpinning model, if one assumes that the dislocation structure responsible for the peaks in curve B is different than that responsible for curve C. Curve D is difficult to explain since the gradual movement of the peak to higher strain amplitude with increasing temperature is a contradiction of thermally assisted unpinning theories.

If the breakaway peak damping height above background ( $\Delta_{\text{BAP}}$ ) is plotted as a function of temperature, as done in fig. 4.12, several important features emerge.  $\Delta_{\text{BAP}}$  decreases

as one goes through the low strain amplitude peak region (500 - 650°C) and this decrease tends to co-incide with the return of the breakaway peak to higher strain amplitude at these temperatures.  $\Delta_{BAP}$  is given by breakaway theories to be given by:

$$\Delta_{BAP} = K_0 \rho L_n^4 \quad 4.5$$

where:  $L_n$  is the network loop length,  $\rho$  the dislocation density and  $K_0$  is a constant. Therefore, for a gradual decrease in  $\Delta_{BAP}$ , either  $\rho$  or  $L_n$  would have to decrease gradually. It seems unlikely, however, that a decrease in the density of dislocation is responsible since annealing of dislocations, although possible at these temperatures (500 - 650°C), would be small over the time span the measurements were taken in. It seems then that  $L_n$  the network loop length is decreasing in this temperature region. The fact that this shortening of  $L_n$  is taking place in the temperature region of the low amplitude relaxation peak suggest the effects are related. A shortening of the network loop lengths could conceivably reduce the average pinned loop lengths and would cause the breakaway peak to move to higher critical stress or strain amplitude which is what is observed in our experiments (fig. 4.12)

Thus, the movement of the strain amplitude dependent peaks to higher strain amplitude with higher temperature which seems to be a contradiction of thermally assisted unpinning theories can be explained in light of the apparent reduction in network loop lengths.



If the relaxation of dislocation predicted by Worrigard's model as presented earlier, is responsible for the low-amplitude peak; this relaxation may be related to the change in  $\ln$ . The actual relationship is not clear but several possibilities exist. Upon becoming unpinned, a dislocation undergoing climb as well as glide as predicted by Worrigard's model, may become dissociated and the dislocation outside the plane of glide may be free to move and interact with other dislocations. Thus, new dislocations are generated which may act as new network pinning points, shortening the network loop length.

It is also possible that the climbing portions of the dislocation may become so large at higher strain amplitudes in the unpinned state that they interact with other dislocations, undergoing the same process in a manner which shortens  $\ln$ , i.e. through pinning. However, any further elaboration on the actual mechanism will have to await further experimental tests.

Amplitude dependent effects in the grain boundary peak area of magnesium has been reported by Smith and Leak<sup>23</sup>. The amplitude dependent damping curves are somewhat similar to the ones obtained by us on the low amplitude side of the peaks. No peaks were detected in Smith and Leak's experiments, which may only be because the strain range investigated was not sufficient to reveal peaks in magnesium.

## 5. CONCLUSIONS AND SUGGESTIONS FOR FURTHER WORK

1. The L.T.P. in zirconium and zirconium alloys has been shown to be very sensitive to thermal heat treatments. The grain diffusion controlled viscous boundary sliding model cannot account for this effect without variation in grain size. A dislocation model involving the reversible climb and glide of dislocations in a lattice network can be used to explain this phenomena.
2. Strong amplitude dependence in the region of the L.T.P. has been observed. This effect can be explained by a dislocation unpinning model similar to that of Granato & Lucke.
3. The number of breakable pinning points per dislocation obtained was approximately 8. This number was calculated using an extension of the Granato & Lucke theory to high strain amplitudes modified by Ritchie et al. Although the number 8 is reasonable for the number of pins, the calculation may be only a lower limit, due to possible interference in the high strain amplitude side of the peak from an increasing background.
4. The movement of the strain amplitude dependent damping peaks to lower strain amplitude with temperature can be explained by the thermally assisted unpinning model. However, the movement to higher strain amplitudes with increasing

temperature can be explained only by a reduction of the network loop lengths  $L_n$ . Further evidence of a reduction in loop lengths in this temperature region,  $L_n$  was obtained by a decrease in the dislocation unpinning peak heights in the same temperature region. The temperature region of this apparent reduction in  $L_n$  coincides with the relaxation peak at low strain amplitude. Therefore, it is postulated that the effects are related, and several possible explanations were advanced using an extension of a dislocation relaxation model similar to that presented by Worrigard in his thesis.

5. If the model developed in this paper is a general one for L.T.P. in zirconium, one should see the same general effect in single crystals of marz grade material. A low strain amplitude peak in damping should occur in the same approximate temperature position in single crystals as in polycrystalline materials as long as the same dislocation structure exists. Accompanied with this peak should be the same type of characteristic unpinning strain amplitude peaks.

6. A L.T.P. in damping at low strain amplitude has been observed in single crystal F.C.C. materials<sup>22</sup>, slightly strained. A similar experiment should be carried out on zirconium with particular attention being given to amplitude dependent damping in the L.T.P. region.

REFERENCES

1. T.S. Kê, Phys. Rev. 70, 105(A) (1946)
2. C. Zener, Phys. Rev. 60, 906 (1941)
3. T.S. Kê, Phys. Rev. 71, 533 (1947)
4. T.S. Kê, Phys. Rev. 72, 41 (1947)
5. R. Raj and M.F. Ashby, Met. Trans., 2, 1113 (1971)
6. D.R. Mosher and R. Raj, Acta Meta., 22, 1469 (1974)
7. R.C. Griffins, Mat.Sci. Eng., 2, 181 (1967)
8. J.T.A. Roberts and P. Barrand, Trans. TMS - AIME, 96, 172 (1968)
9. Leak, G.M. Proc. Phys. Soc., 78, 1520 (1961)
10. J. Worrigard, Thèse
11. Bratina and Winegard
12. Gacougnolle, Thèse Poitress France (1974)
13. K.W.S. Sprungmann and I.G. Ritchie A.E.C.L. 3794 Whiteshell Nuclear Research Centre (1971)
14. J. Putman, I.G. Ritchie and F.J. Hughes Whiteshell Nuclear Research, A.E.C.L. 3953 (1972)
15. N.F. Mott, Proc. Phys. Soc., 60, 391 (1948)
16. G.W. Miles and G.M. Leak, Proc. Phys. Soc., 77, 1529 (1961)
17. J.T.A. Roberts, Mel. Trans., 1, 2487 (1970)
18. R. Raj and M.F. Ashby, Met. Trans., 3, 1937 (1972)
19. J. Weertman, J. Appl. Phys., 26, 1213 (1955)
20. Y. Ishida and D. McLean, (1967), J. Meta. Sci., 1, 171
21. M.F. Ashby, Scripta - metall., 3, 843 (1969)

22. Y. Ishida and S. Liu Conference at Asilomas, U.S.A. on "The Strength of Metals and Alloys" (American Society for Metals) (1970)
23. C.C. Smith and G.M. Leak, Sixth Conf. I.F., 1, 383 (1975)
24. G. Schoek, E. Bisgoni and J. Shyne, Acta. Met., 12, 1466 (1964)
25. I.G. Ritchie, H.E. Rosinger and A. Atrens (to be published)
26. Granato and K. Lucke, J. Appl. Phys., 27, 789 (1956)
27. K. Lucke and J. Schlipf, Conf. on the Interaction Between Dislocations and Point Defects, Harwell, p. 118 (1968)
28. D.G. Blair, T.S. Hutchison, and D.G. Rogers, Canadian Journal of Phys. 48, 2955 (1970)
29. D.H. Rogers, Journal Appl. Phys., 33, 781 (1962)
30. I.G. Ritchie, A. Atrens, and C.H. Woo (to be published)

### Figure Captions

- Fig. 2.1 - Relaxation of an initially uniform shear stress distribution by grain boundary sliding.
- Fig. 2.2 - Sliding by elastic accommodation results in an-elasticity. The rate of sliding is controlled by diffusive accommodation of sliding across the particles.
- Fig. 2.3 - Spring dashpot model representing the Raj and Ashby model for I.F. due to impurities at grain boundaries.
- Fig. 2.4 - Dislocation bowing out through a combination of glide and climb as predicted in the model of Worrigard.
- Fig. 3.1 - The torsion pendulum instrumentation.
- Fig. 3.2 - The torsion pendulum and vacuum chamber.
- Fig. 3.3 - Typical Micrographs.
- Fig. 3.4 - Curve A is the experimental damping spectrum taken from the X - y plotter (specimen #4). Curve B is the subtracted background. Peaks C and D are the resulting curves after background subtraction.
- Fig. 3.5 - The top dotted curve is a plot of  $\ln(\Delta)$  vs.  $1/T$  using the data of curve A of fig. 2.4. The straight line is the extrapolated background which transforms to curve B of fig. 2.4.
- Fig. 3.6 - Curve A is the experimental damping spectrum for specimen 1 after an in situ anneal at  $780^{\circ}\text{C}$ . Curve B is the background, and D and C are the resulting peaks.
- Fig. 3.7 - A is the experimental spectrum for damping, and B is the background, and C the resolved peak before in situ anneal. D, E, F, and G are similar curves but after an in situ anneal for the Zr-Mo-0 (specimen #3).
- Fig. 3.8 - Damping spectrum for Zr-Y-0 (specimen #4) at 1.68Hz, A, B, and C are as indicated before.
- Fig. 3.9 - Damping spectrum for Zr-Y-0 (specimen #4) at .554Hz. A, B, and C are as indicated before.

- Fig. 4.1 - Reed Pendulum apparatus. - detail
- Fig. 4.2 - Reed Pendulum apparatus. - schematic
- Fig. 4.3 - Strain amplitude dependent damping curves taken from free decay of specimen #5 in the temperature range of 413°C to 493°C.
- Fig. 4.4 - Strain amplitude dependent damping curves taken from free decay of specimen #5 in the temperature range of 512°C to 580°C.
- Fig. 4.5 - Strain amplitude dependent damping curves taken from free decay of specimen #5 in the temperature range of 596°C to 644°C.
- Fig. 4.6 - Strain amplitude dependent damping curve (solid line) and modulus defect  $M$  given by equation 3.1 (dotted line). All taken at 550°C.
- Fig. 4.7 - A is the curve obtained from damping at nominal strain amplitude 1 in figs. 3.3, 3.4, and 3.5. B, C, and D are the strain amplitudes for maximum damping ( $\Delta_{BAP}$ ) from figs. 3.3, 3.4, and 3.5.
- Fig. 4.8 - Amplitude dependent damping curves for specimen #4.
- Fig. 4.9 - The lower curve is the damping at nominal strain amplitude of 1 for specimen #4. The top curve is strain amplitude at  $\Delta_{BAP}$  (approximate).
- Fig. 4.10- A Granato-Lucke plot of  $\ln(\Delta_{BA}\epsilon)$  as a function of  $1/\epsilon$ .
- Fig. 4.11- A plot of  $\Delta_{BA}$  as a function of  $1/\epsilon^2$  for high strain amplitudes.
- Fig. 4.12-  $\Delta_{BAP}$  is plotted with the nominal 1 strain amplitude curve and strain amplitude at  $\Delta_{BAP}$  in the region of the L.T.P. of fig. 3.7.

<u>No.</u>	<u>Specimen</u>	<u>Method of Test</u>	<u>Grain Size* Before Testing (mm)</u>	<u>Grain Size* After (mm)</u>
1.	Zr (Marz Grade)	Torsion	.076	.084
2.	Zr-.1wt/%Y-1.wt/%O	Torsion	.0605	.049
3.	Zr-1.wt/%Mo-1.wt/%O	Torsion	.026	.026
4.	Zr (Marz Grade)	Reed	-	.162
5.	Zr (Marz Grade)	Reed	-	.063

\*determined by the intersection method

Table 1

Element	O	H	Fe	HF	Al	Cl	Mo	Y
μg/g	30.0	16.0	30.0	200.0	10.0	15.0	1.0	1.0

Table 2



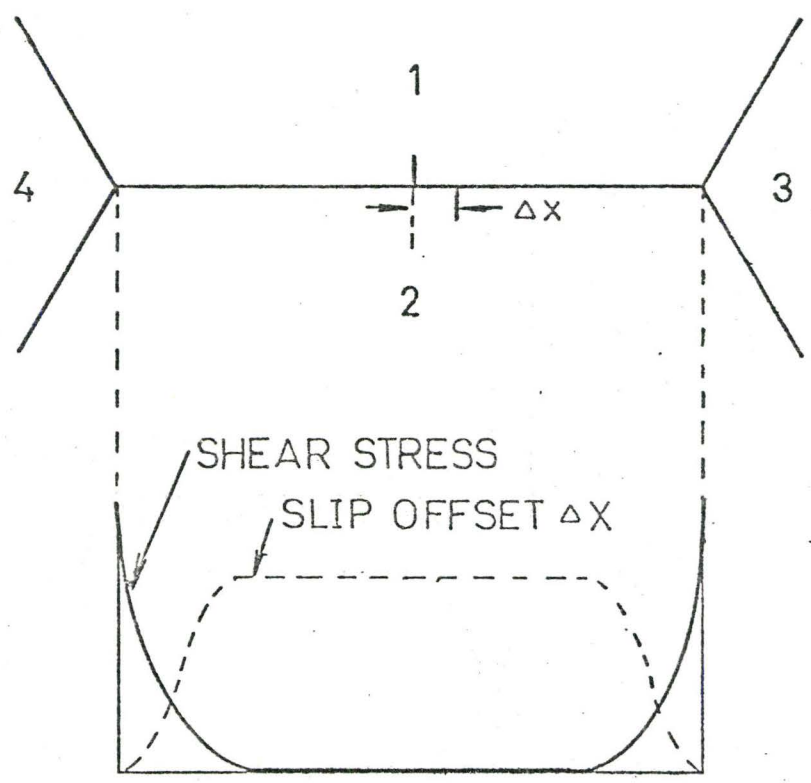


Fig. 2.1

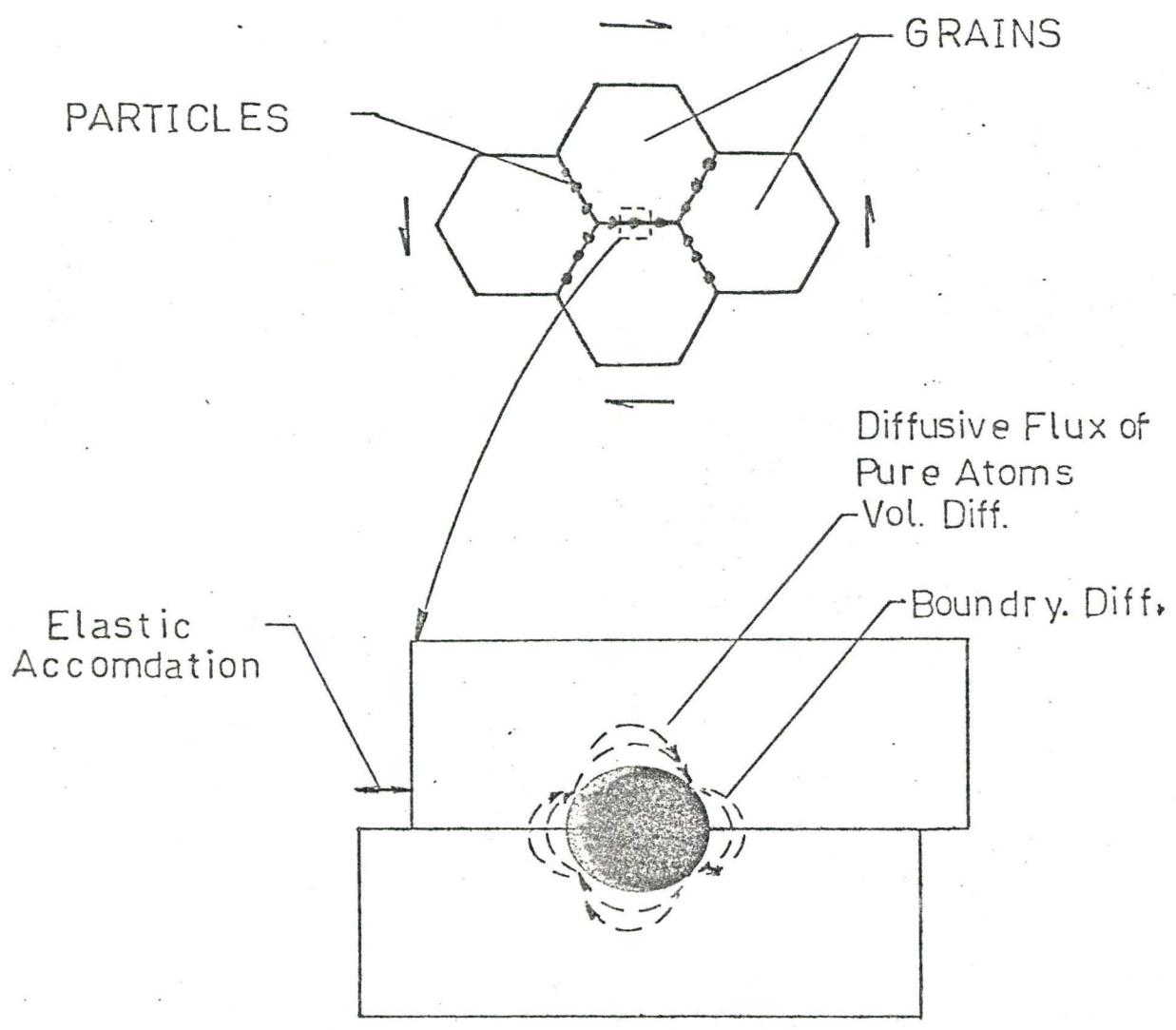


Fig. 2.2

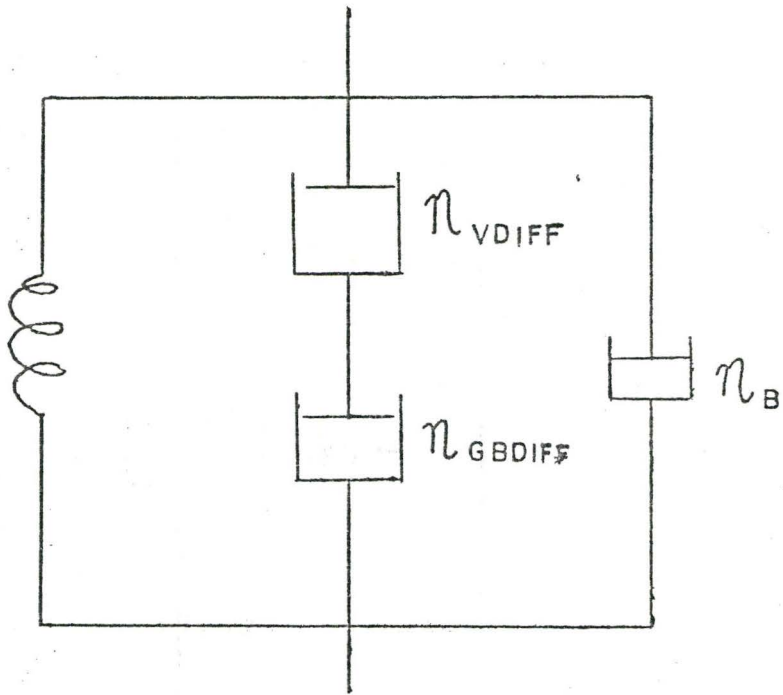


Fig. 2.3

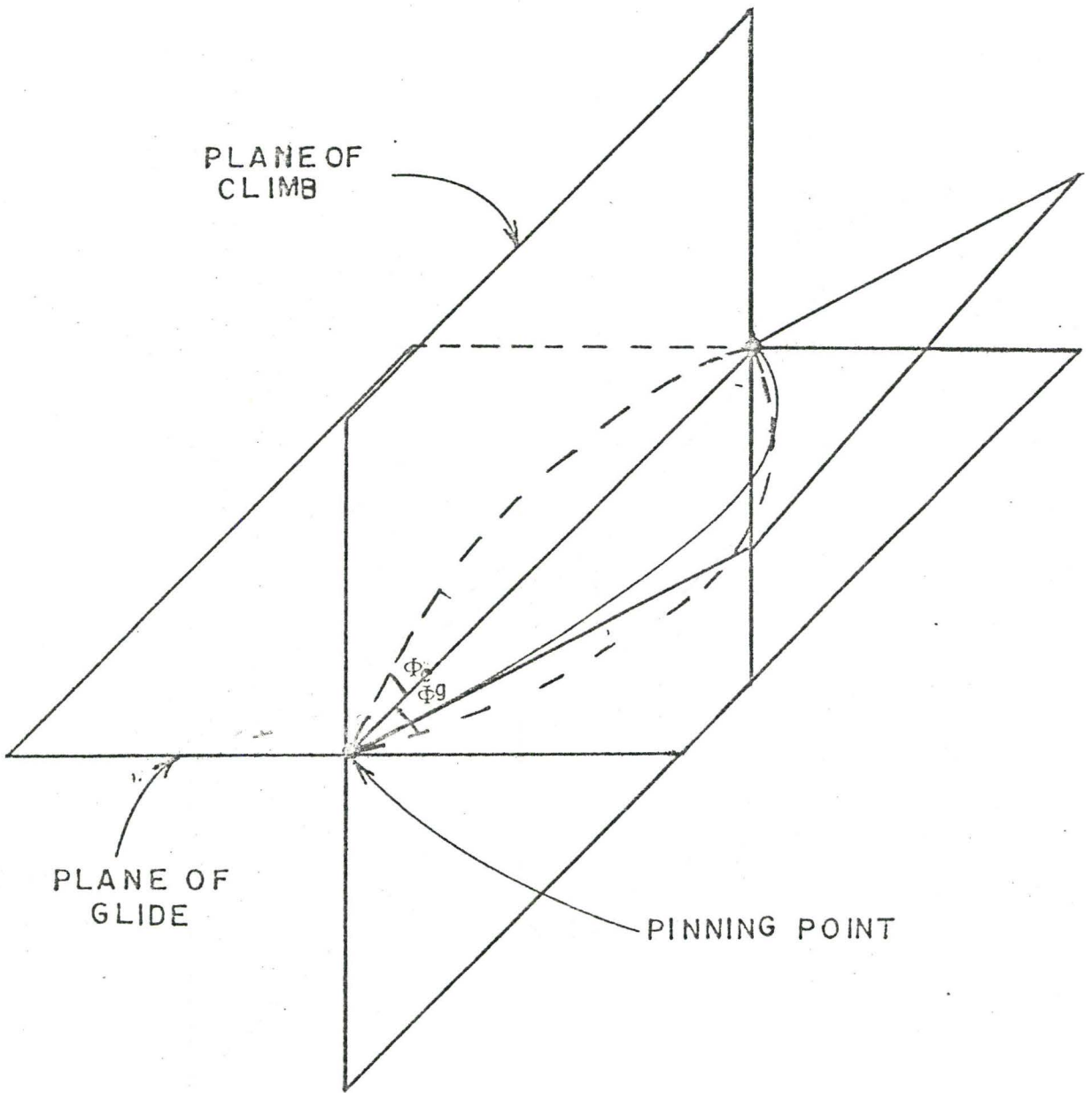
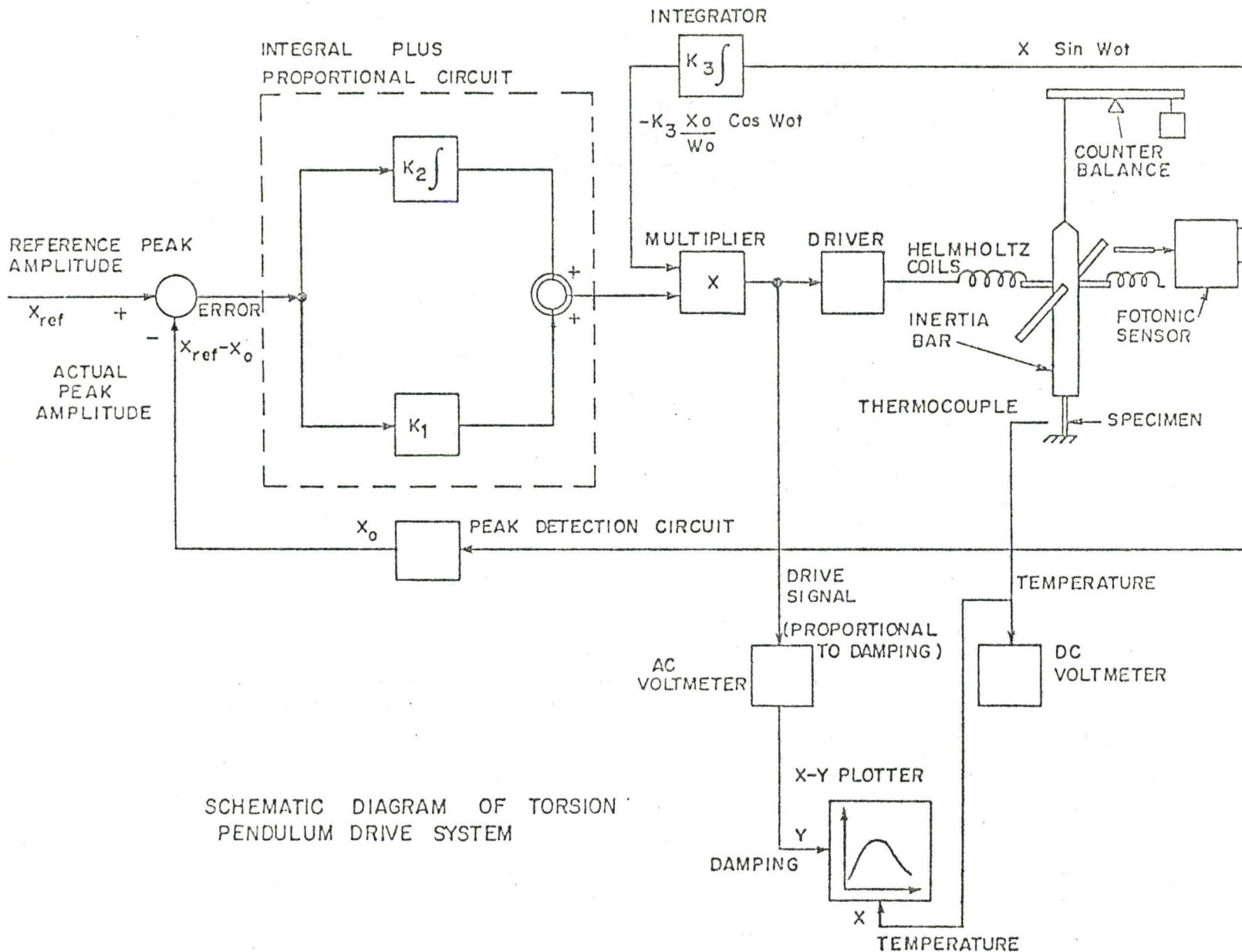


Fig. 2.4



SCHMATIC DIAGRAM OF TORSION PENDULUM DRIVE SYSTEM

Fig. 3.1

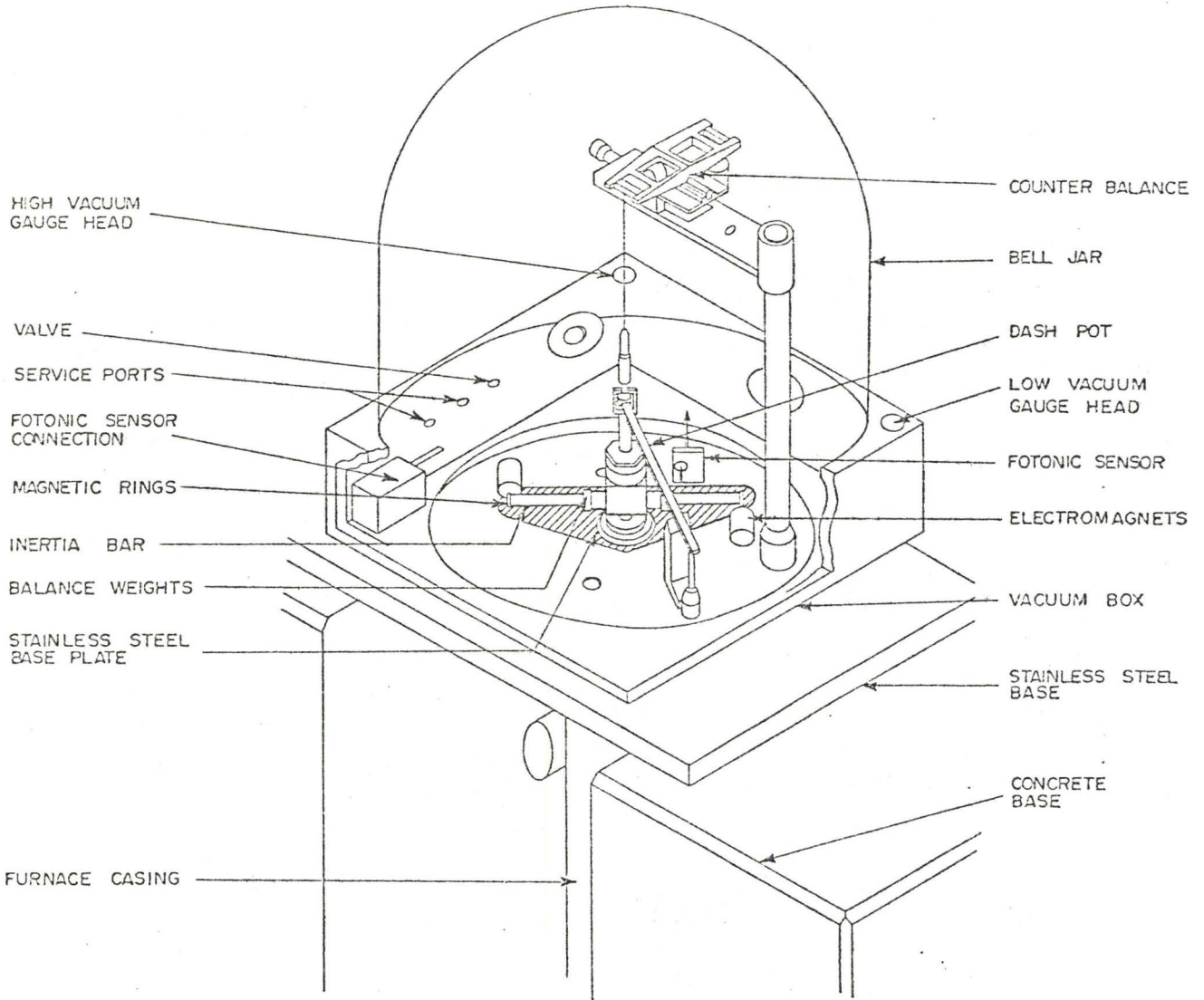
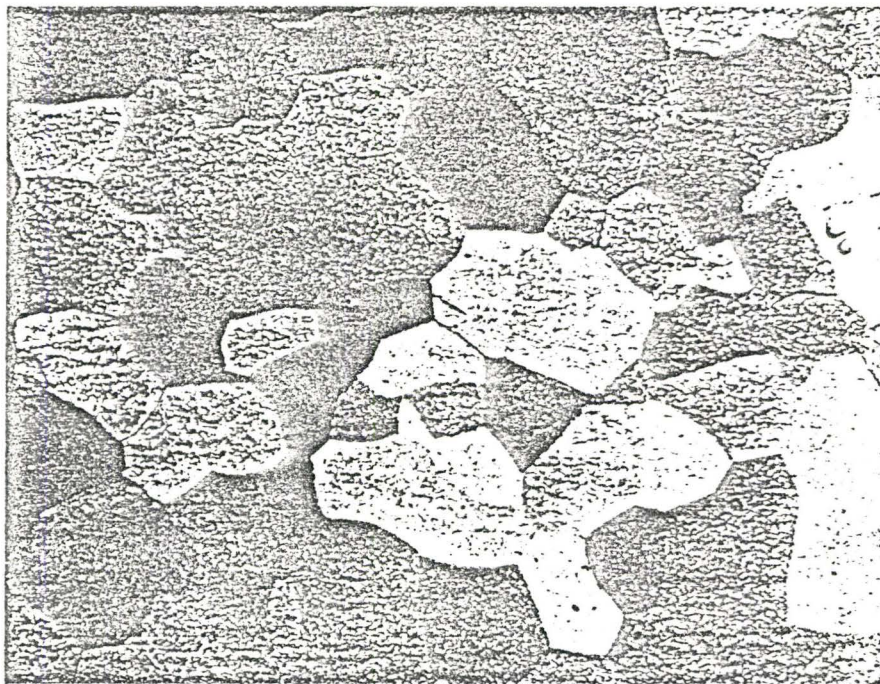


Fig. 3.2



Before testing



After testing

Fig. 3.3

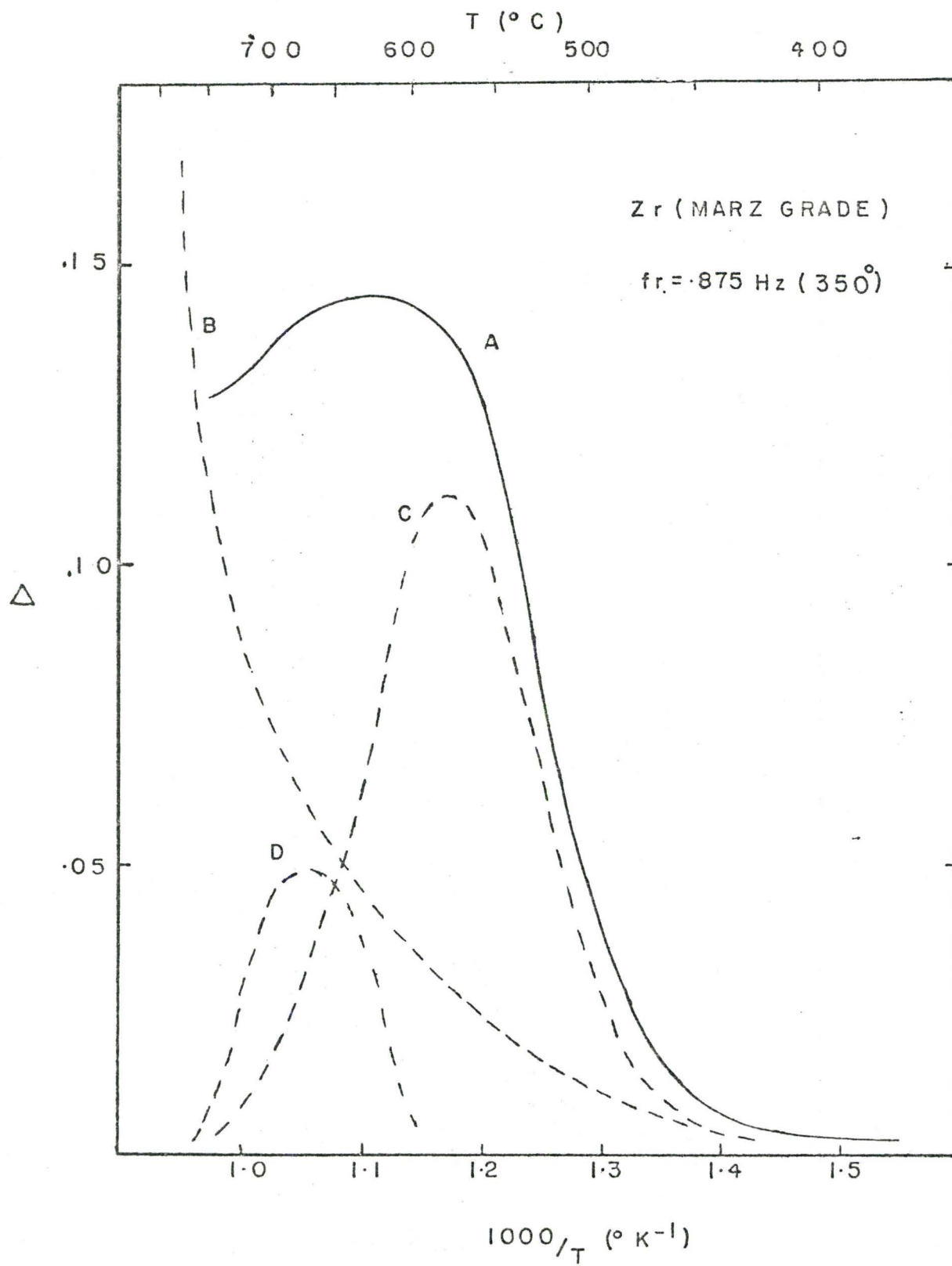


Fig. 3.4



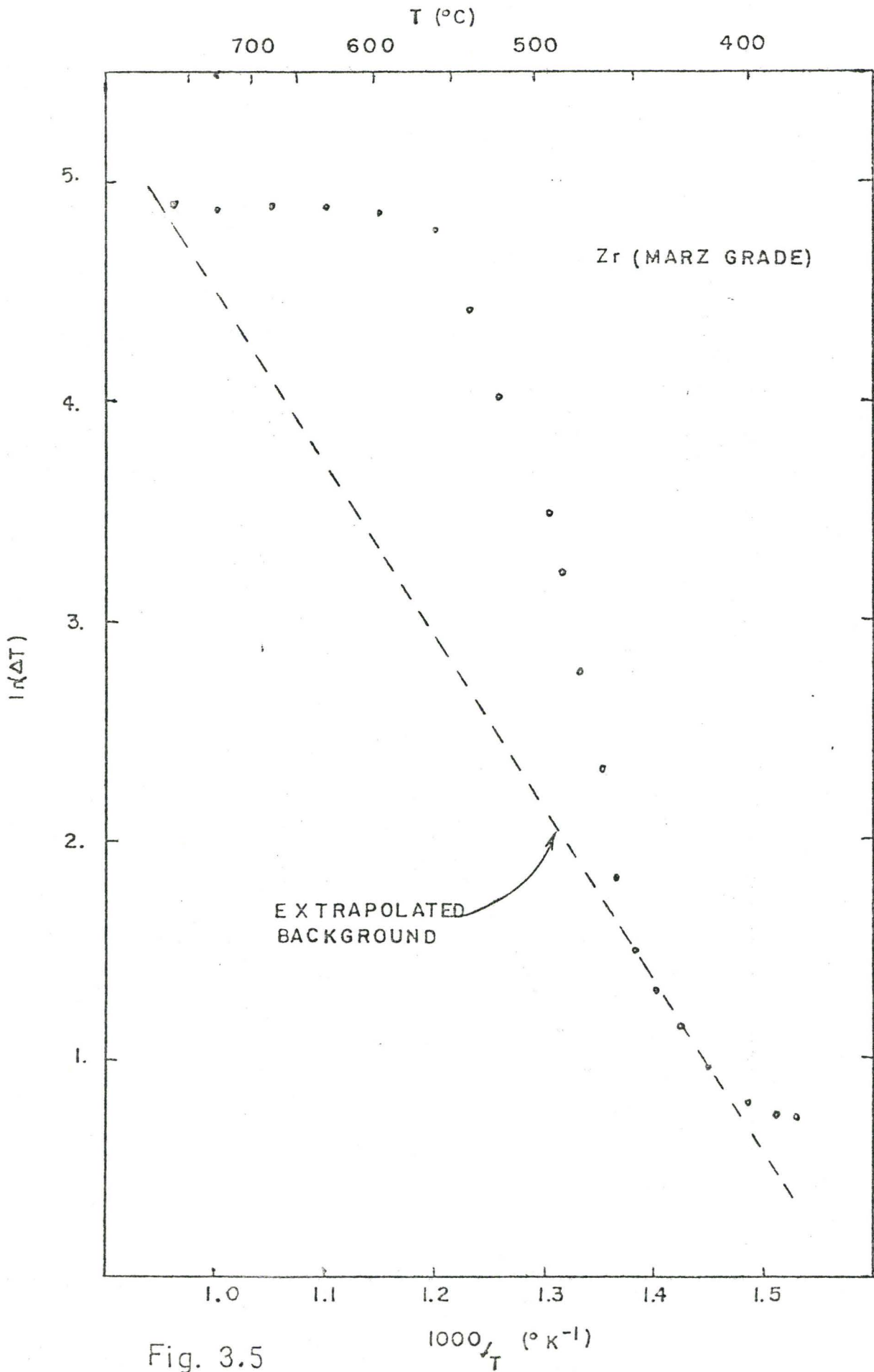


Fig. 3.5

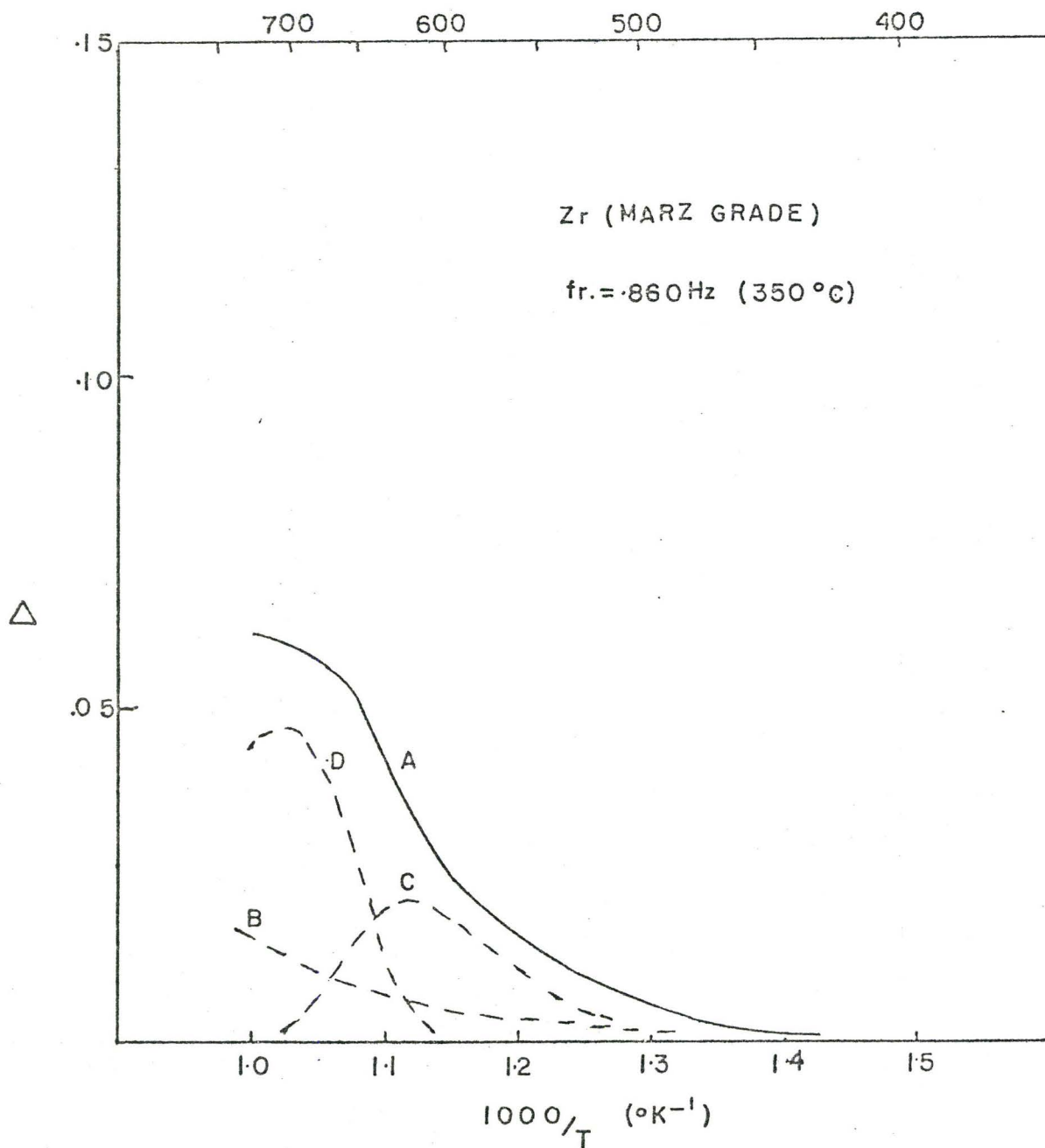


Fig. 3.6

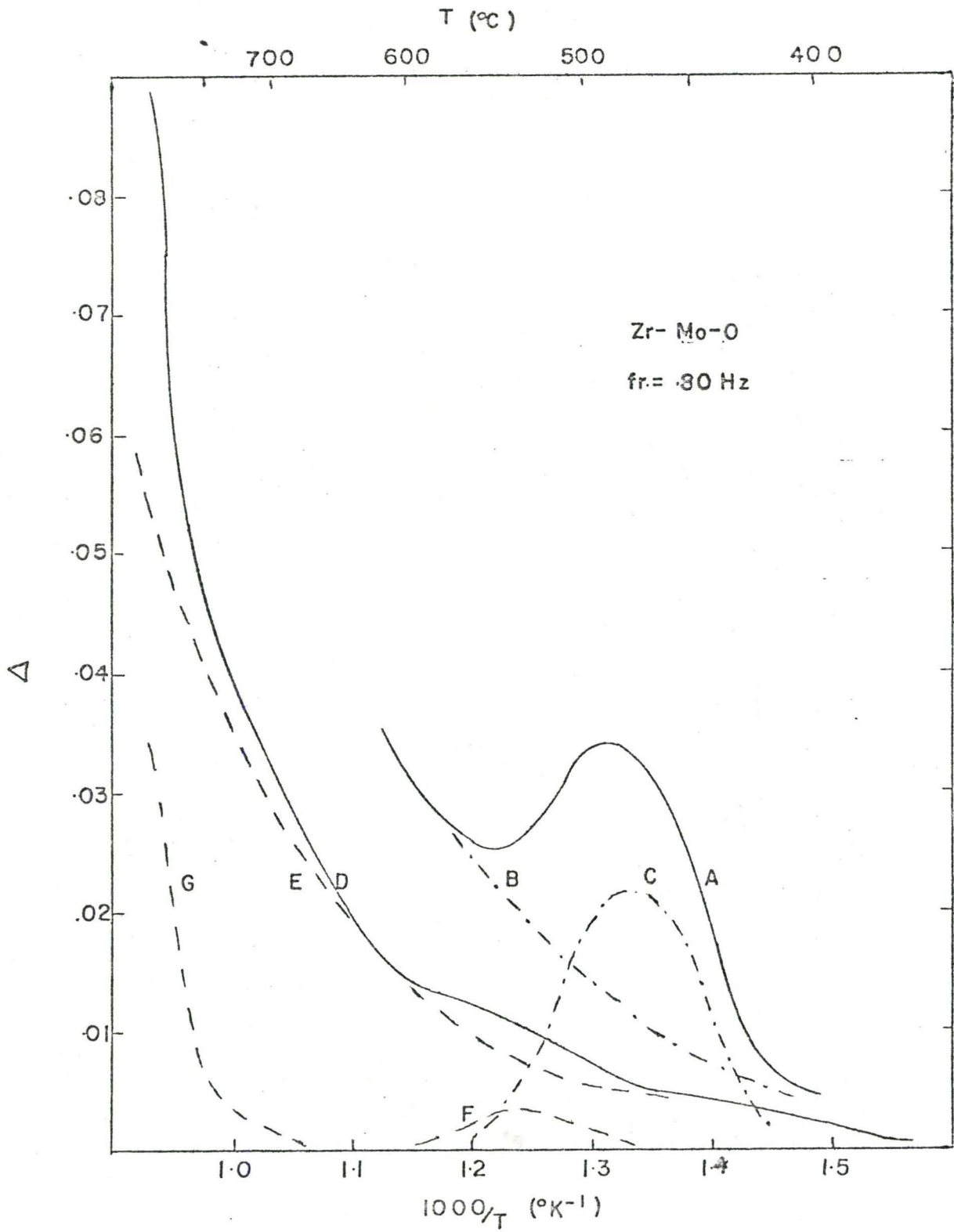


Fig. 3.7

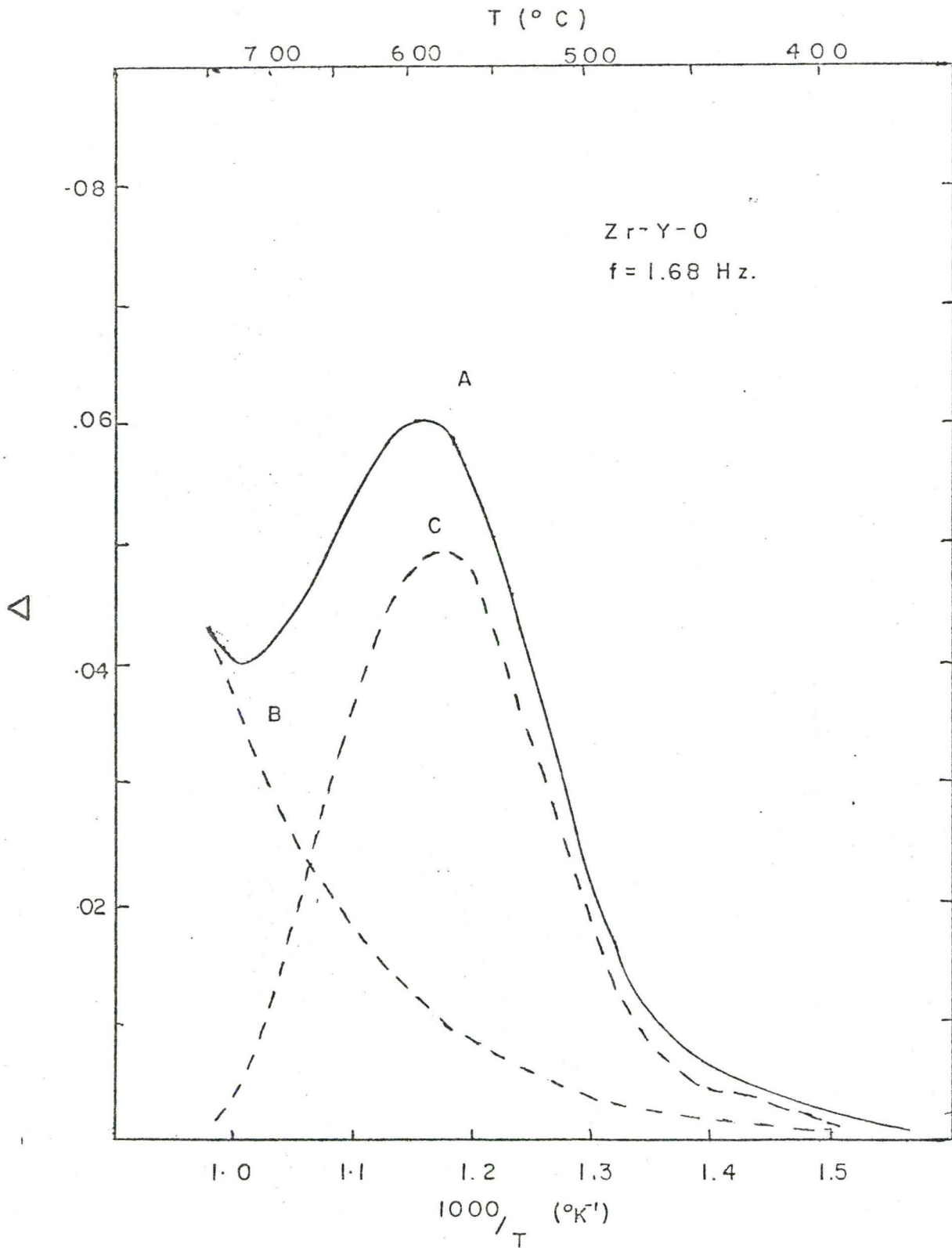


Fig. 38

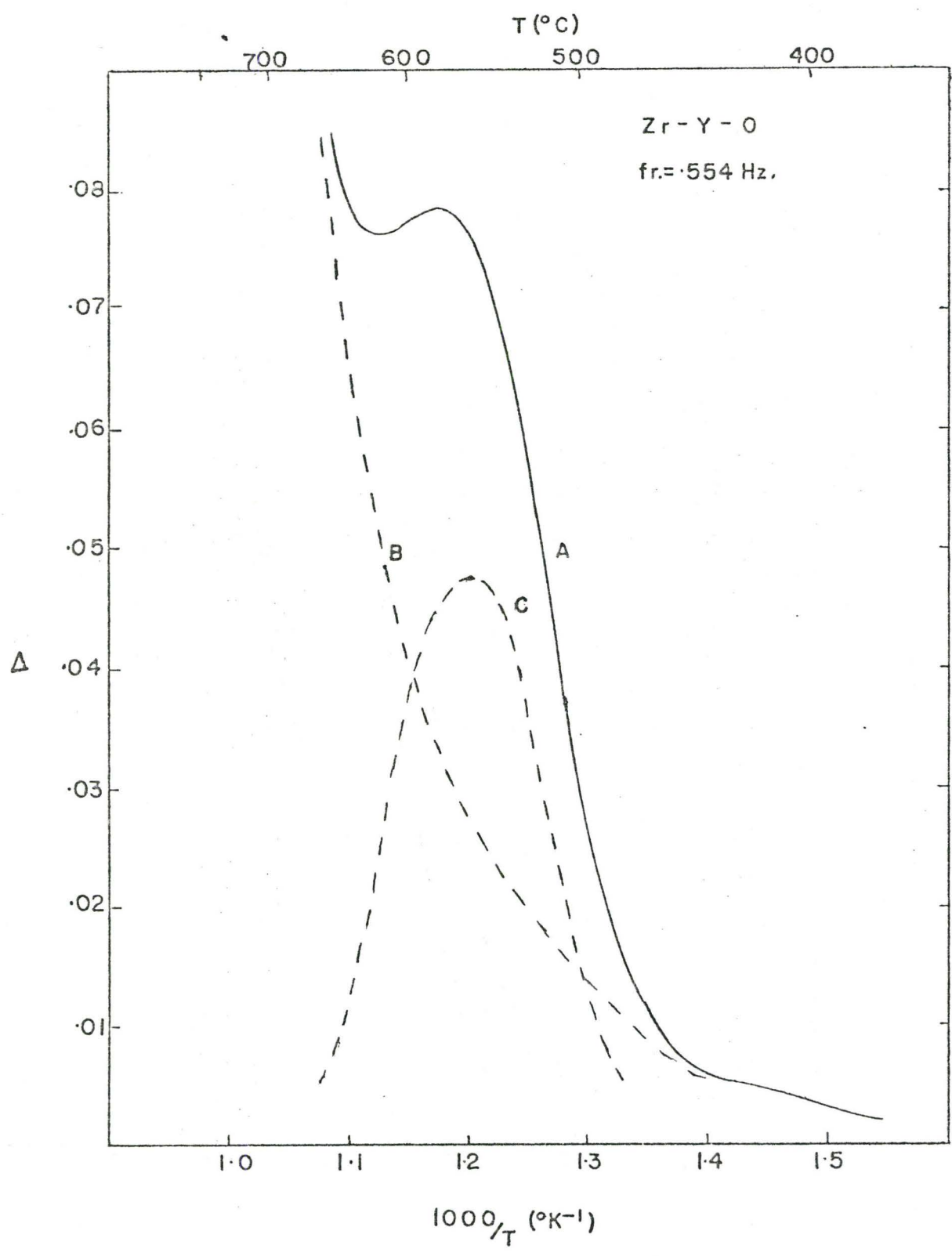


Fig. 3.9

## KEY TO FIGURE

- A. Specimen
- B. Pendulum Rod Assembly
- M. Lava Base
- N. Wedges for Lower Grips
- O. Collar for Lower Grips
- P. Main Heater
- Q. Auxiliary Heater
- R. Temperature Equalizer
- S. Thermocouples
- T. Quartz Plate
- U. Heat Shield

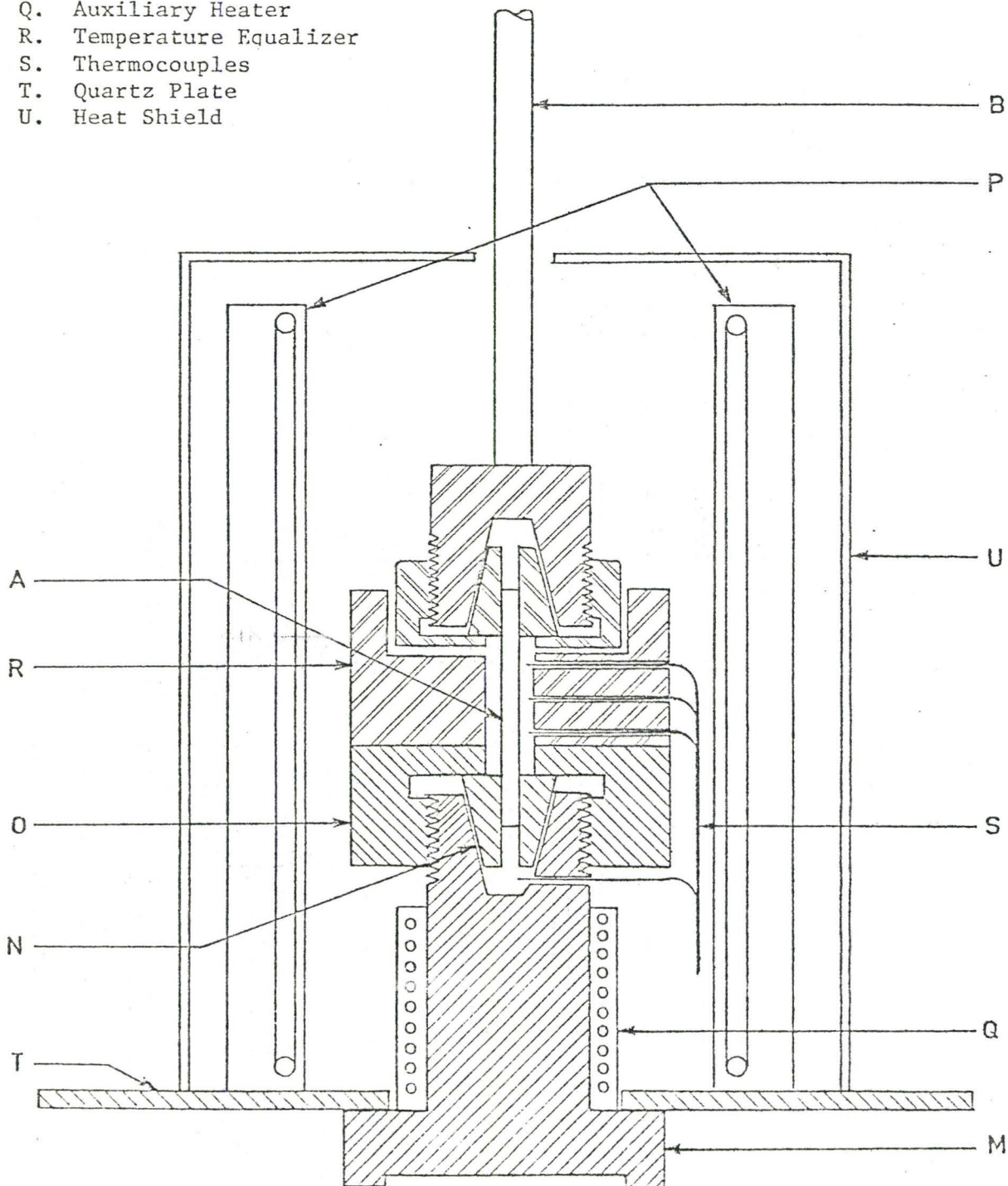


FIGURE 4.1 Reed Pendulum - Detail

KEY TO FIGURE

- A. Specimen
- B. Pendulum Rod Assembly or Inertia Member
- C. Soft Iron Plug
- D. Reflecting Surface for Fotonic Sensor (Transducer)
- E. Electromagnet
- F. Fotonic Sensor Probe
- G. Base Plate
- H. Stanchion
- J. Electromagnetic Shelf
- K. Transducer Shelf (Fotonic Sensor)
- L. Bell Jar (Vacuum Chamber)
- M. Lava Base
- P. Main Heater
- Q. Auxiliary Heater
- R. Temperature Equalizer
- U. Heat Shield
- V. Cooling Jacket for Fotonic Sensor Cartridge

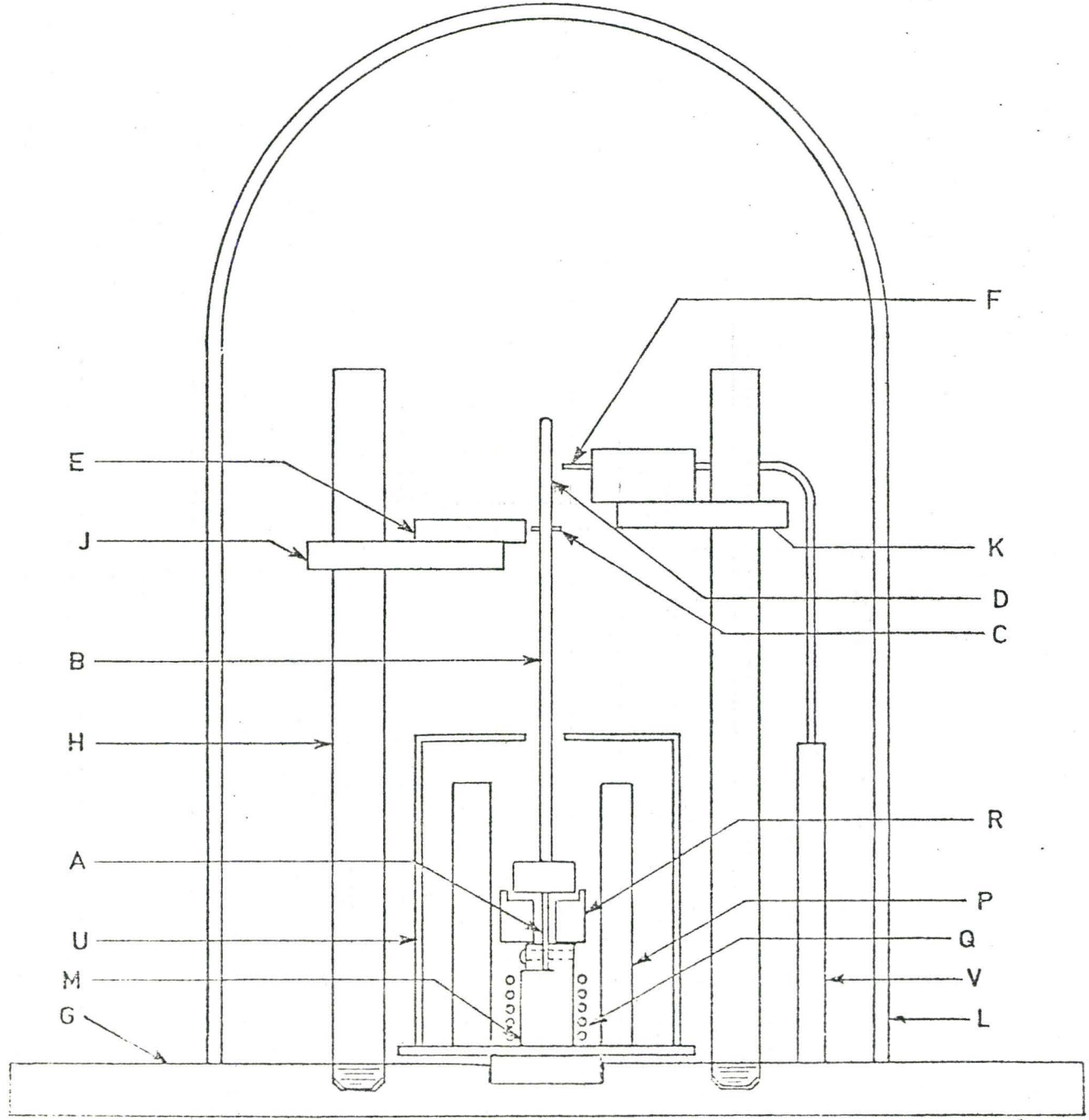
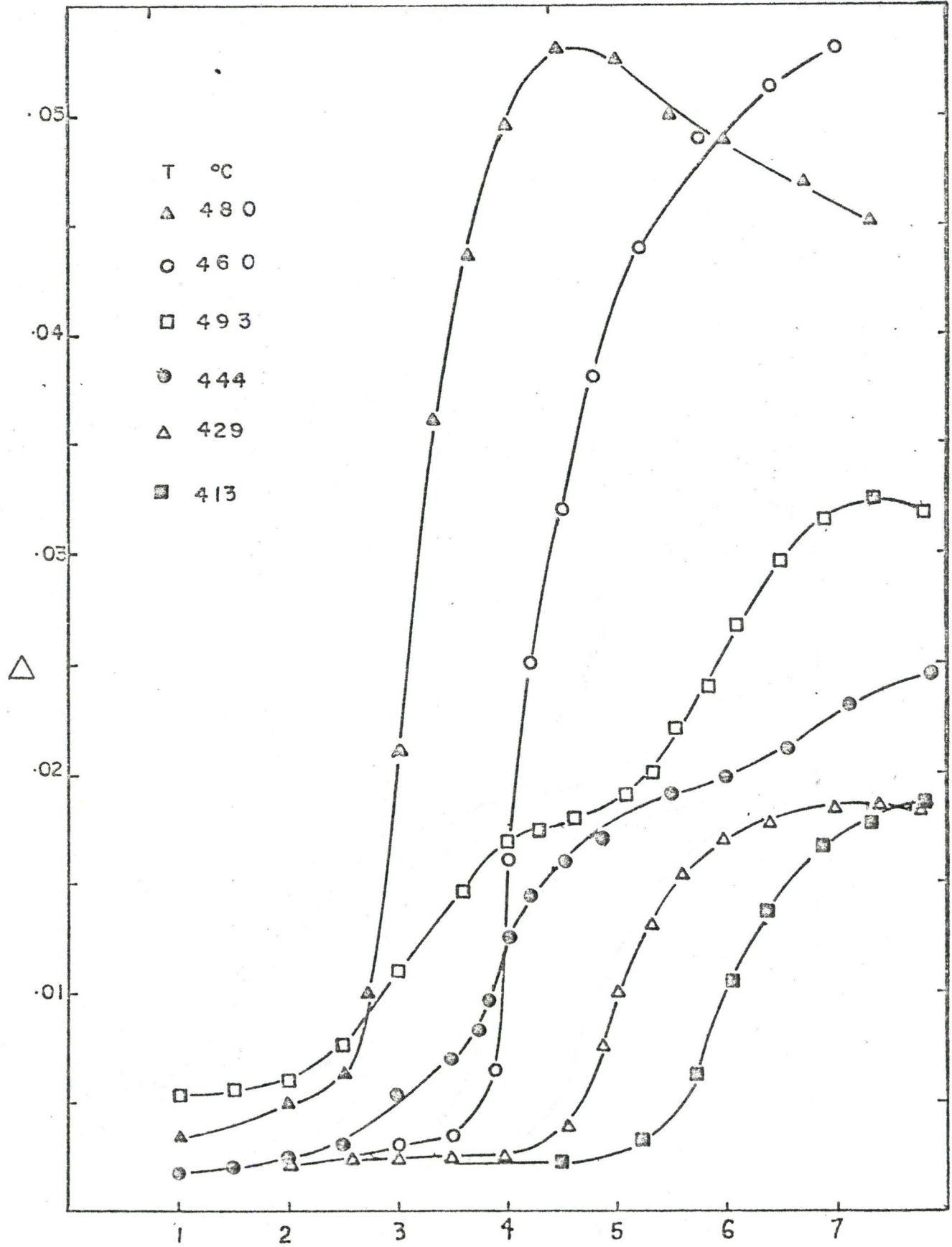


FIGURE 4.2 Reed Pendulum - Schematic

$\epsilon (\times 10^6)$   
5.0

1.0

10.



(NOMINAL STRAIN AMPLITUDE

Fig 4.3



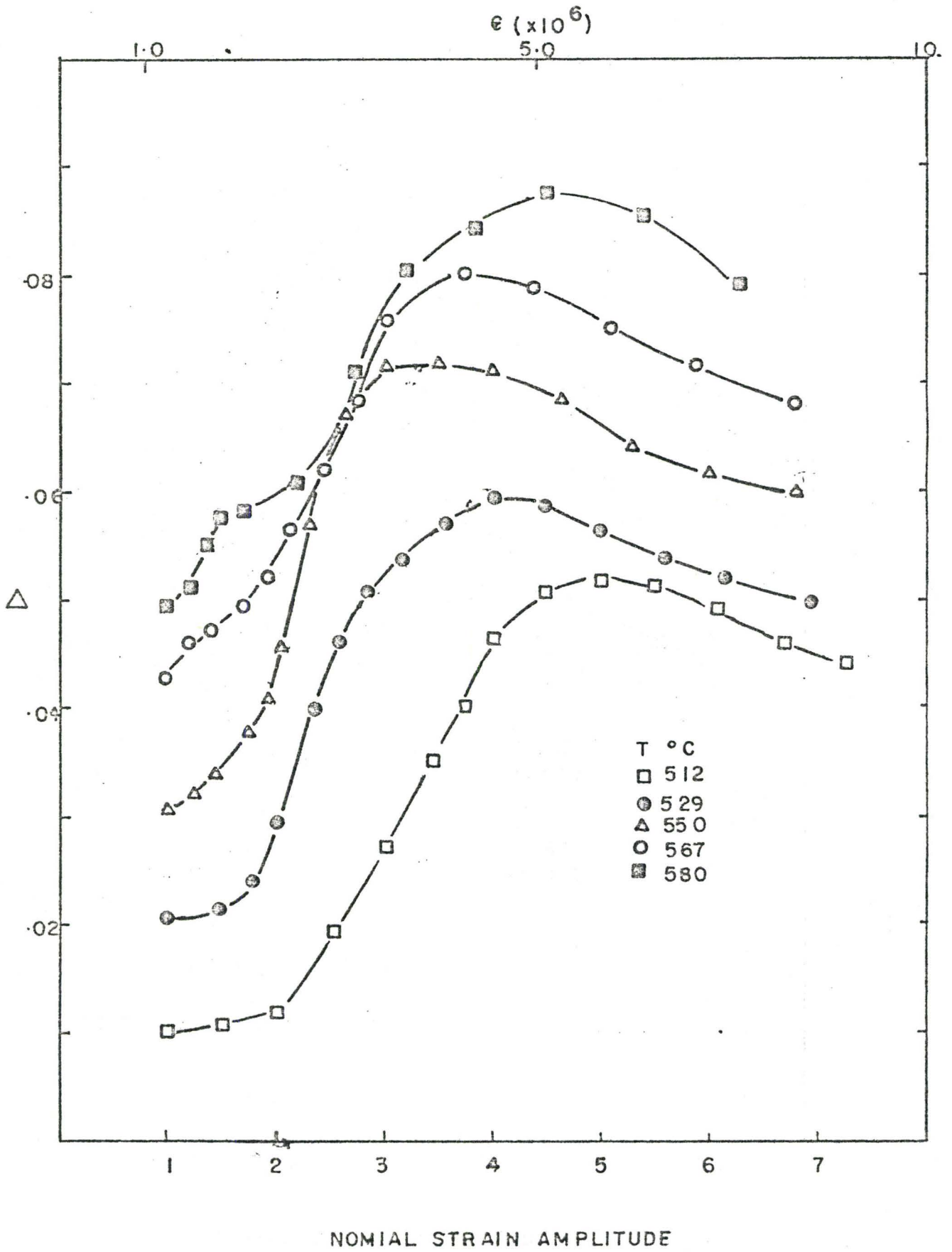


Fig. 4.4

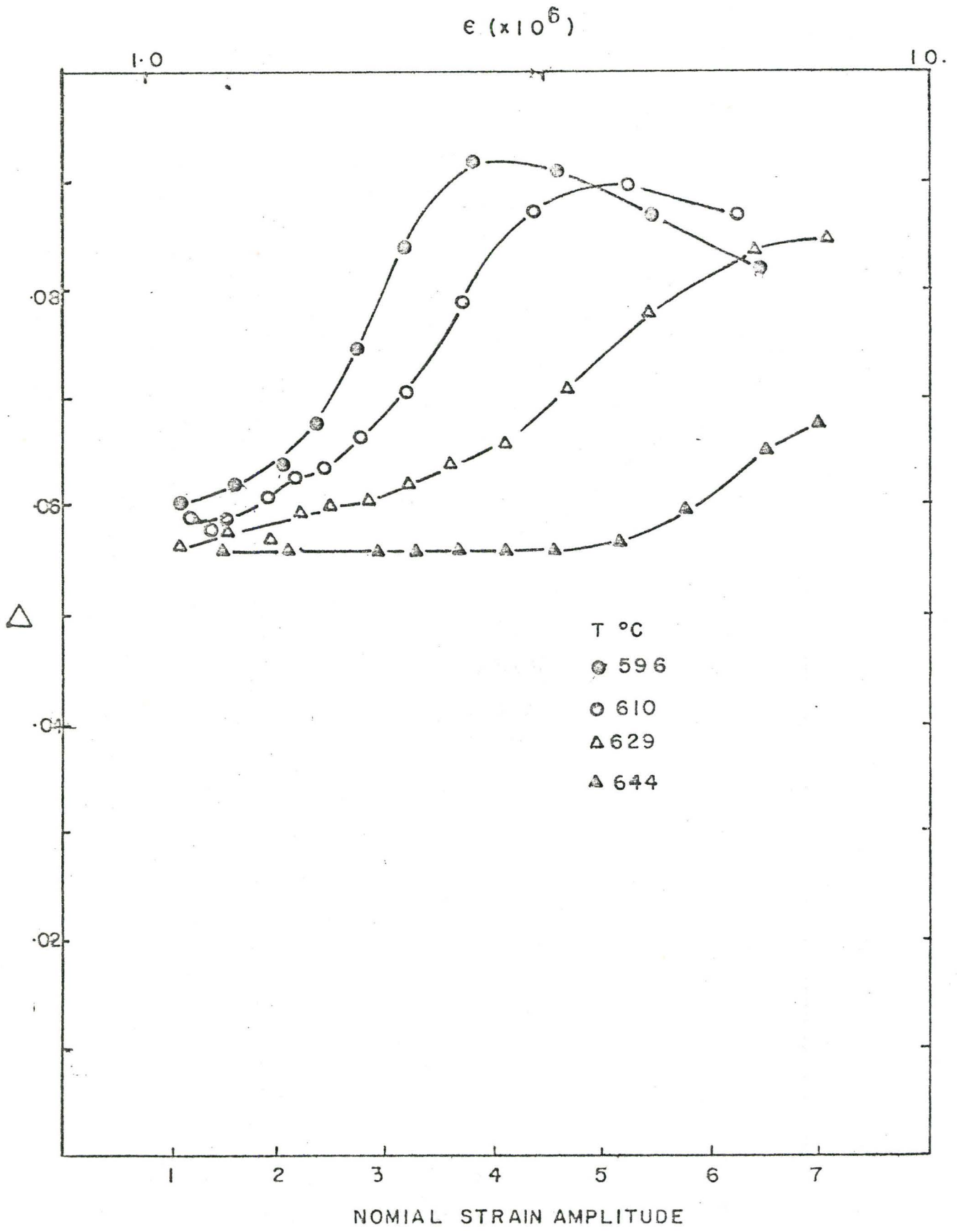


Fig. 4.5

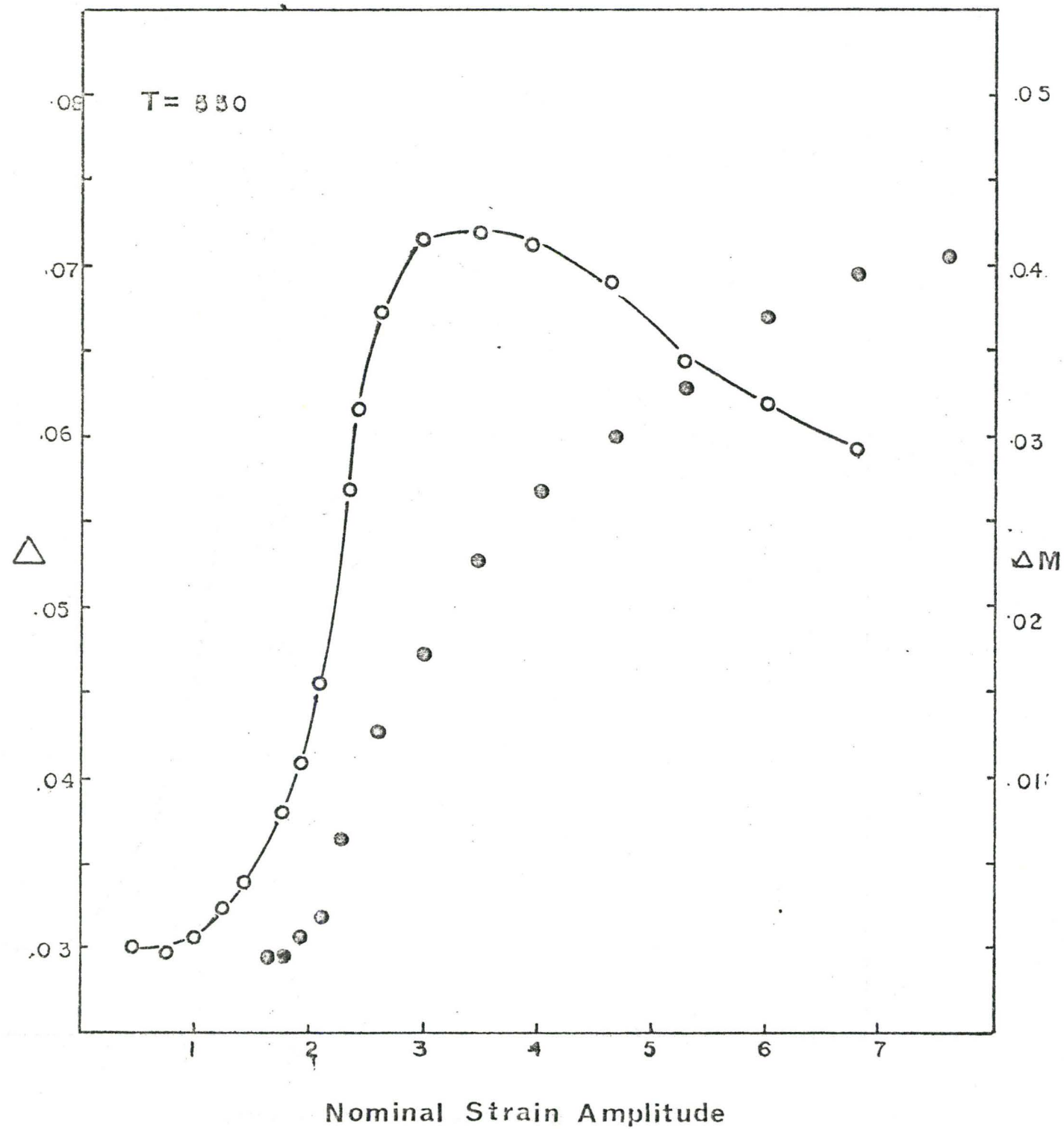


Fig. 4.6

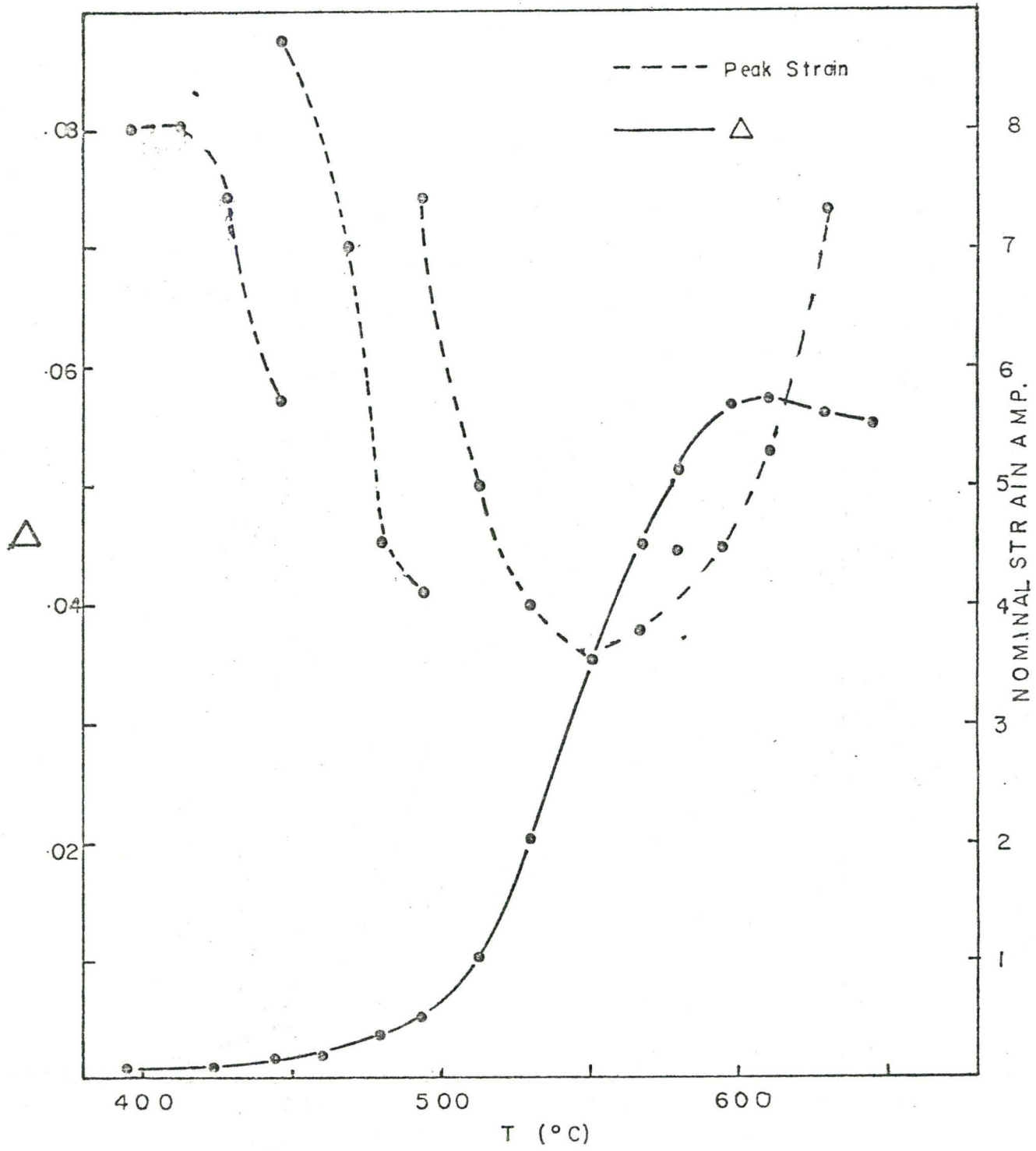


Fig. 4.7

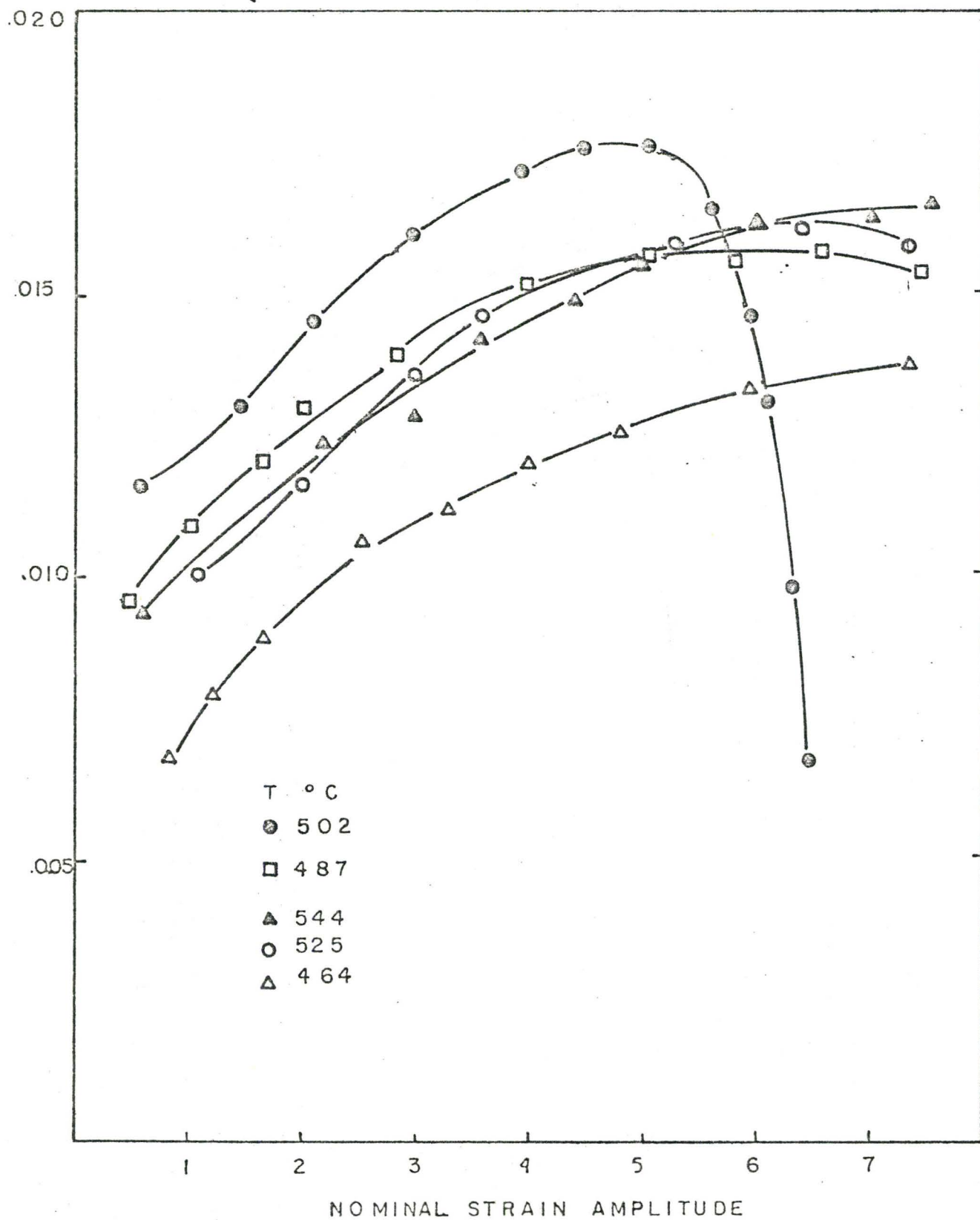


Fig.4.8

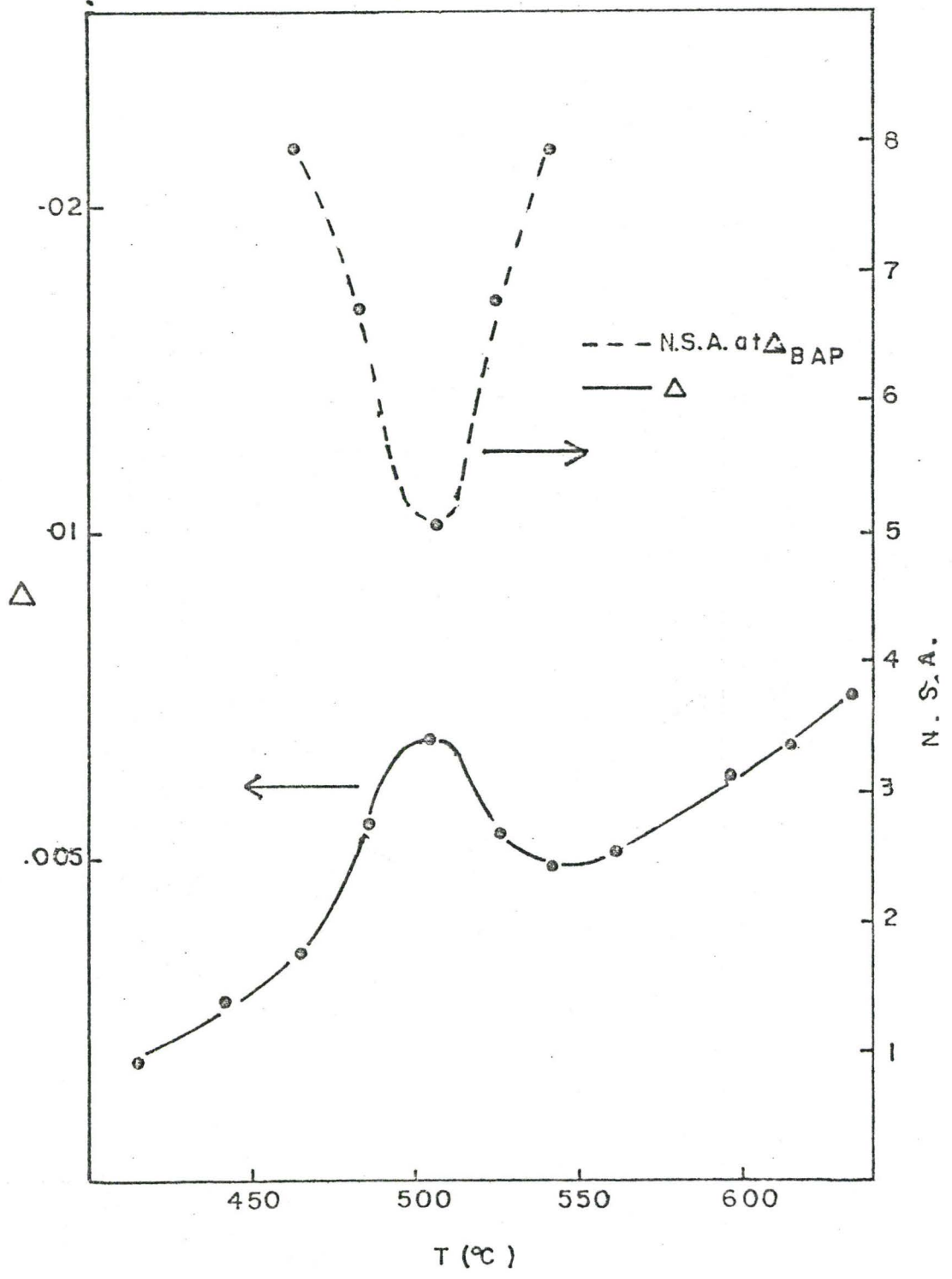


Fig. 4.9

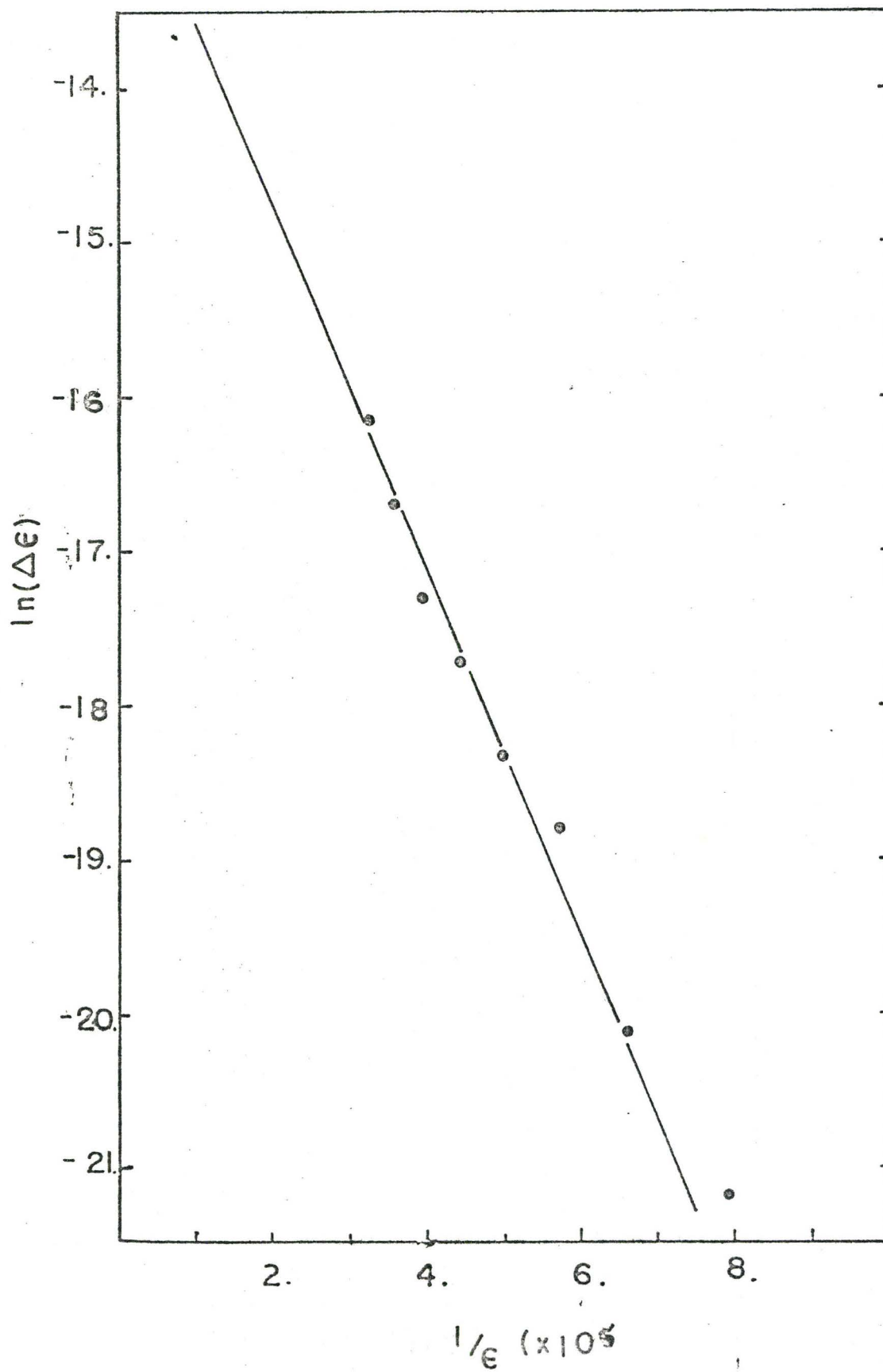


Fig. 4.10

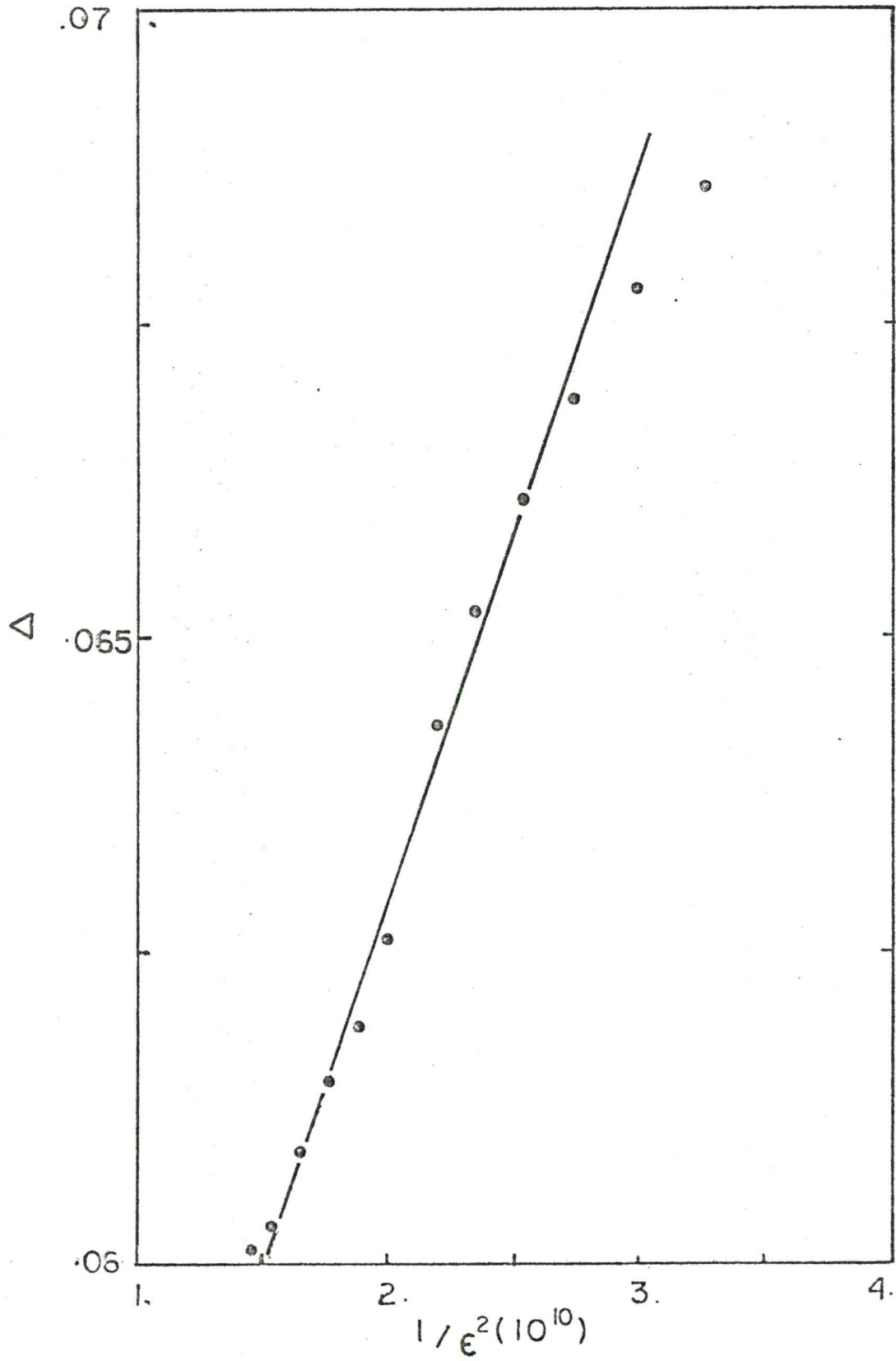


Fig. 4.11